Thesis for the Degree of Master of Engineering

High Performance Control of
Permanent Magnet Synchronous Motor

By

Sun Quanbin

Department of Mechatronics Engineering

The Graduate School

Pukyong National University

February 2012

High Performance Control of

Permanent Magnet Synchronous Motor

영구자석형 동기모터의
고성능 제어법에 관한 연구

Advisor: Professor Seok-Kwon Jeong
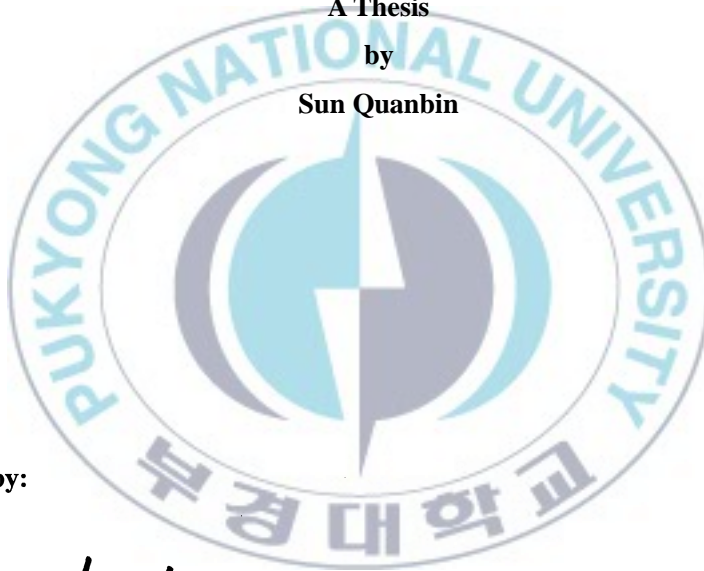
By
Sun Quanbin

A Thesis submitted in partial fulfillment of the requirements

for the degree of

Master Degree

In the Department of Mechatronics Engineering

The Graduate School,

Pukyong National University

February 2012

High Performance Control of
Permanent Magnet Synchronous Motor

A Thesis
by
Sun Quanbin

Approved by:

Joo-Ho Yang
(Chairman)

Ji-SungJang   Seok-Kwon Jeong
(Member)   (Member)

December, 2011

Abstract

Permanent Magnet Synchronous Motor(PMSM) appeared at the 1950s century. Accompany with the development of power electronic technology and micro-computer at the 1970s century, PMSM starts to be applied in high performance speed control systems. At the 1980s century, the development of PMSM had been greatly facilitated by the development of rare earth permanent magnet materials has break through, especially the turn up of 3rd generation new rare earth permanent magnet material neodymium iron boron(NdFeB) which with high residual magnetism, strong coercivity and low price. Thus the control performance of PMSM also had qualitative leap. From then on, AC permanent magnet speed control system gradually replaced the traditional DC speed control system, to be used widely in various high performance motion control systems, and become an important branch in AC speed control field.

This thesis emphatically introduced the vector control system of BLACM and torque ripple rejection strategy of BLDCM, and explained two types of pulse-width modulation (PWM) technology. At last, established BLACM vector control system and BLDCM control system by using MATLAB/SIMULINK, and implemented simulation.

In this study, BLACM vector control experiments of two PWM algorithms were completed by programming with CCStudio software, based on TI DSP(TMS320F28035) control board. The experimental results show that there is good control effect for BLACM with vector control algorithm. By comparing the waveforms of line voltage and phase current, SVPWM algorithm is better than SPWM algorithm in switch loss and harmonic content.

From the BLDCM torque ripple suppression simulation result, it is effective to reduce the ripple of BLDCM torque with dual closed-loop BLDCM control algorithm based on CHBPWM technology.

Contents

List of Figures

List of Tables

Nomenclatures

u_d	Voltage in d axis	V
u_q	Voltage in q axis	V
i_d	Current in d axis	A
i_q	Current in q axis	A
p_n	Pole pair number	
ψ_d	Flux linkage in d axis	Wb
ψ_q	Flux linkage in q axis	Wb
L_d	Inductance in d axis	H
L_q	Inductance in q axis	H
R_s	Armature resistance	Ω
ψ_r	Permanent magnet flux linkage	Wb
T_e	Electromagnetic torque	Nm
T_L	Load torque	Nm
J	Moment of inertia	Kg m^2
P	Differential operator	
u_a, u_b, u_c	Phase voltage	V
i_a, i_b, i_c	Phase current	A
e_a, e_b, e_c	Back emf	V

L	Self-inductance of winding	H
M	Mutual inductance of winding	H
T_r	Torque ripple (%)	
T_{max}	Maximum electromagnetic torque	Nm
T_{min}	Minimum electromagnetic torque	Nm
T_N	Average electromagnetic torque	Nm
e_m	The amplitude of back emf	V
i_m	The amplitude of phase current	A

Chapter 1

Introduction

1.1 Background

PMSM uses anti-degaussing permanent magnet rotor to replace winding rotor, so as to overcome the fatal disadvantage of AC synchronous servo motor by eliminating the electric brush of winding rotor motor. Meanwhile, it has advantages such as small size, light weight, low inertia, high efficient, no heating of rotor, etc.

At the present, the output power range of PMSM is high up to 1000kW, and low to microwatt grade. It is not only covered the power range of micro, small and middle size motors, but also extends to large power field. Since 1980s, because of its excellent performance of high torque to inertia ratio, high power density, high efficient, etc, PMSM had been widely used in middle and small volume range. Nowadays, the usage of PMSM in military field is dominated, almost replaced all electromagnetism motors. And PMSM has been used widely in daily life, such as driving system of new energy automobile, numerically controlled machine tools and precise machine tool, air conditioning system, etc.

Foreseeable, along with the further price reduction of high field permanent magnet and continuously perfection and improvement of motion control theory & technology, PMSM and its driving system will have further development and application.

1.2 Review of the previous studies

In 1971, engineer F.Blaschke of Siemens company in German came up with "induction motor field-oriented vector control theory" which introduced the theory foundation for high performance control. Vector control theory had firstly been applied in induction motor control with ideal control effect. Later, people tried to apply vector control theory into BLACM control, and got even better control performance. Meanwhile, vector control was easier to realize in BLACM control. Besides, accompany with the appearance of new permanent magnet material, the power density of BLACM increased greatly. So nowadays, BLACM vector control system are used in most high performance servo driving systems, such as numerical control machine, robot, etc.

1.3 Objective and outline of the present study

This thesis studied the high performance control technology of two types of PMSM separately. Main contents are as below:

1.3.1 High performance control of BLACM

1. Firstly, in this study, the mathematical model of BLACM is studied, and the modularization design and simulation of BLACM control algorithm are completed with MATLAB.

2. Sinusoidal Pulse Width Modulation (SPWM) and Space Vector Pulse Width Modulation (SVPWM) are the two types of pulse width modulation technologies which been mostly used in AC motor control. This thesis has done detailed theoretical explanation about SPWM and SVPWM, and completed the simulation of two types PWM technology in MATLAB, as well

as compared their simulation results.

3. The BLACM vector control experiment based on TI DSP control board is completed by programming with C language in CCStudio(Code Composer Studio) software environment.

1.3.2 High performance control of BLDCM

1. In this study, the constitution and working principle of BLDCM control system are introduced detailedly.

2. The reasons and reduction method of BLDCM torque ripple are studied deeply, and the simulation model of BLDCM control system is completed with MATLAB.
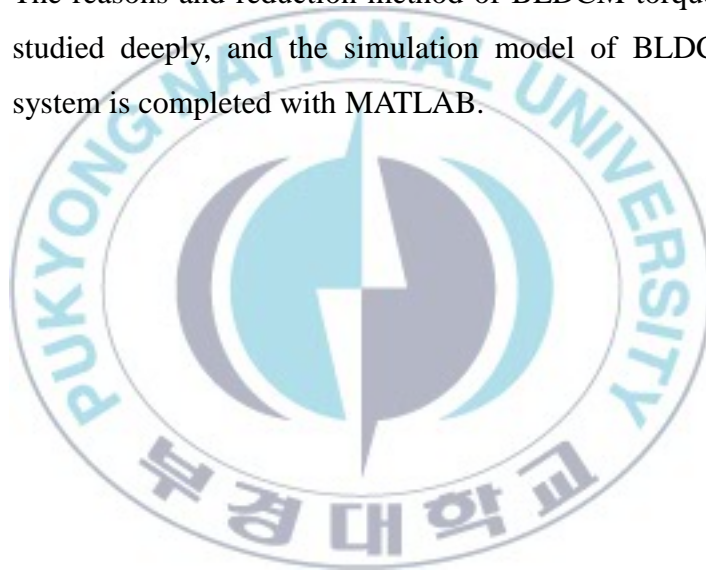
Chapter 2

Study of theory

2.1 Features of PMSM

PMSM uses permanent magnet to generate air-gap field, rather than commutator motor which using magnet exciting coil to generate air-gap field, neither like induction motor which using the flux components of stator current to generate air-gap field. Its advantages include simple structure, low consumption, and high efficient.

The rotors of PMSM are mostly made by rare earth permanent magnet material. Because the geometry shape of rotor magnets is different, the distribution of rotor field in space is divided as sine wave and trapezoidal wave. Meanwhile, when the rotors rotating, the back emf wave form generated on stator also divided as two types: one is sine wave, another one is trapezoidal wave.

For distinguishing these two types of PMSM, the back emf wave form as sine wave to be called as brushless AC motor (BLACM), back emf wave form as trapezoidal wave to be called as brushless DC motor(BLDCM). Because the structure BLACM and BLDCM are different, so they are great different in the motor model, control method, constitution of control system and application range.

For generating constant torque, the stator current of BLACM required sine wave symmetric current, while the stator current of BLDCM required square wave current. Because of the inertia of electromagnetism, the actual stator current of BLDCM is trapezoidal wave, not be able to generate square

current. Besides, because of concentrated winding for power supply, the torque pulsation of BLDCM is larger than BLACM. So in high accurate servo systems, BLACM has more competitiveness. But because the moment generated by unit current in BLACM is smaller than which in BLDCM, when driving same volume motor, the volume of inverter required by BLACM is larger, and because the control current of BLACM is sine wave, therefore the consumption when on-off will increase.

Table 2.1 The comparison between two types of PMSM

Compares content	Type of motor	
	BLACM	BLDCM
Power density	Low	Higher 50% than BLACM
Torque inertia	Low	Higher 50% than BLACM
Speed regulation range	Wide	Narrow
Control method	Complex	Simple
Rotor position measure	Continuous measure	60 electric angle detection
Torque Constant	Small	Big
Torque ripple	Small	Big

From Table 2.1, BLDCM has advantages like simple control structure, low cost, simple monitor device, compared with BLACM. But because of the inherent defect of its principle, if without any treat, there are disadvantages of large torque ripple and much iron core additional loss.

Those disadvantages greatly limited the application of BLDCM in high accurate and high performance servo systems. So reduction the torque ripple of BLDCM becomes a hot subject in servo system research nowadays.

2.2 The vector control principle of BLACM
2.2.1 Category and basic structure of BLACM

Similar as AC synchronous motor, classify according to non salient pole and salient-pole, BLACM could be classified into two classes: surface BLACM(SBLACM) and interior BLACM(IBLACM). Figure 2.1 is the sectional drawing of these two BLACM.

(a) SBLACM   (b) IBLACM
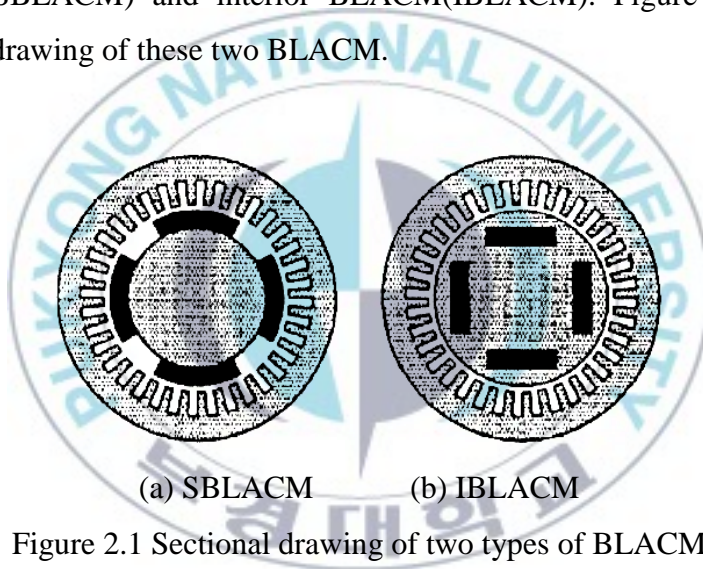
Figure 2.1 Sectional drawing of two types of BLACM

Because the permanent magnet is in the rotor, the SBLACM is able to obtain induced current as soon as possible with small inductance; at the same time, the SBLACM is not able to produce reluctance torque, but with line effects of torque, is suitable for servo system of high speed of answer.

Due to the internal permanent magnet in the rotor, the IBLACM would not allow the magnet to sling out by the overwhelming centrifugal force. IBLACM has better linear torque, thus has a lower manufacturing cost than

SBLACM, and is suitable for servo system of low speed of answer. Rotor of IBLACM does not only produce magnetic torque, but also produce reluctance torque. Higher efficiency can be obtained by flexible application of reluctance torque. Because of this, IBLACM receives more attention.

2.2.2 The coordinate transformation of BLACM
2.2.2.1 The structure of BLACM and coordinate system

Figure 2.2 shows the structure of BLACM. The BLACM stator is composed of three-phase windings and magnetic cores. And the three-phase windings are usually connected by Y-connection. A rotor position sensor is installed to detect magnetic pole position.
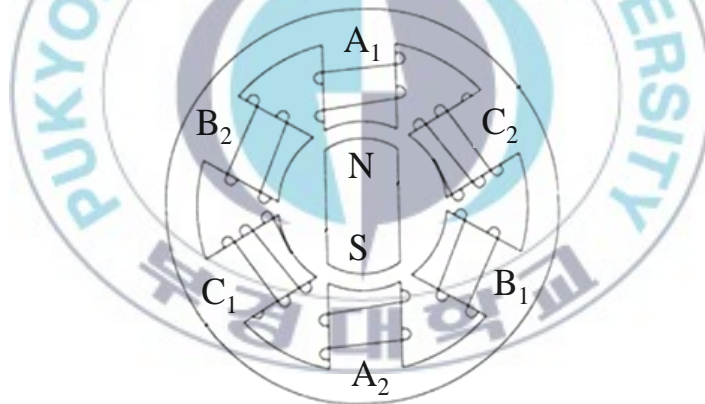
Figure 2.2 Schematic diagram of BLACM structure

The most of vector control is basically based on in the d-q reference model. Three kinds of coordinates, i.e., A-B-C coordinate, α-β coordinate and d-q coordinate, are used in the d-q reference model.

Figure 2.3 represents the three kinds of coordinate systems. In the d-q coordinate system, the magnetic pole is considered as d(direct) axis, and

q(quadrature) axis is leaded 90 degree from d axis. The angel θ is defined as the angle difference between d axis and A axis.
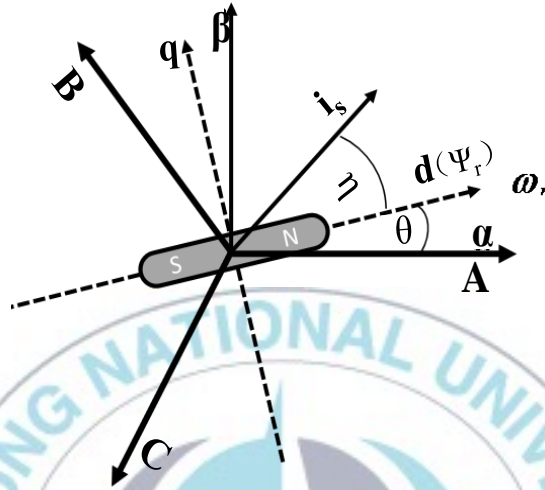
Figure 2.3 Coordinate for vector control of BLACM

As the 3-phase windings are connected by Y connection under the assumption of symmetrical circuit, three-phase currents meet $i_A + i_B + i_C = 0$. And also the power should be constant before and after the coordinate transformation.

Equation (2-1) and equation (2-2) are known as Clarke transformation and inverse-Clarke transformation.

$$\begin{bmatrix} i_\alpha \\ i_\beta \end{bmatrix} = \sqrt{\frac{2}{3}} \begin{bmatrix} 1 & -\frac{1}{2} & -\frac{1}{2} \\ 0 & \frac{\sqrt{3}}{2} & -\frac{\sqrt{3}}{2} \end{bmatrix} \begin{bmatrix} i_A \\ i_B \\ i_C \end{bmatrix} \quad (2\text{-}1)$$

$$\begin{bmatrix} i_A \\ i_B \\ i_C \end{bmatrix} = \sqrt{\frac{2}{3}} \begin{bmatrix} 1 & 0 \\ -\dfrac{1}{2} & \dfrac{\sqrt{3}}{2} \\ -\dfrac{1}{2} & -\dfrac{\sqrt{3}}{2} \end{bmatrix} \begin{bmatrix} i_\alpha \\ i_\beta \end{bmatrix} \tag{2-2}$$

Equation (2-3) and equation (2-4) depict Park transformation and inverse-Park transformation to get d-q currents and α-β currents.

$$\begin{bmatrix} i_d \\ i_q \end{bmatrix} = \begin{bmatrix} \cos\theta & \sin\theta \\ -\sin\theta & \cos\theta \end{bmatrix} \begin{bmatrix} i_\alpha \\ i_\beta \end{bmatrix} \tag{2-3}$$

$$\begin{bmatrix} i_\alpha \\ i_\beta \end{bmatrix} = \begin{bmatrix} \cos\theta & -\sin\theta \\ \sin\theta & \cos\theta \end{bmatrix} \begin{bmatrix} i_d \\ i_q \end{bmatrix} \tag{2-4}$$

2.2.2.2 Mathematical model of BLACM in d-q axis

The d-q reference model is the most popular when we design BLACM vector controller and analyze its dynamic behaviors. Usually there are four equations in the mathematical model of BLACM in the d-q reference model such as the voltage equation (2-5), the stator flux linkage equation (2-6), the electromagnetic torque equation (2-7), and the mechanical movement equation (2-8). These equations can be expressed as following from equation (2-5) to equation (2-8) under the d-q coordinate system.

$$\left. \begin{aligned} u_d &= p_n \psi_d - \psi_q \omega_r + R_s i_d \\ u_q &= p_n \psi_q - \psi_d \omega_r + R_s i_q \end{aligned} \right\} \tag{2-5}$$

$$\left. \begin{array}{l} \psi_d = L_d i_d + \psi_r \\ \psi_q = L_q i_q \end{array} \right\} \tag{2-6}$$

$$\begin{aligned} T_e &= p_n \left(i_q \psi_d - i_d \psi_q \right) \\ &= p_n \left[\psi_r i_q + \left(L_d - L_q \right) i_d i_q \right] \end{aligned} \tag{2-7}$$

$$\frac{J}{p_n} \cdot \frac{d\omega_r}{dt} = T_e - T_L \tag{2-8}$$

2.2.3 Rotor field-oriented vector control

This thesis also established high performance BLACM control system by using field-oriented vector control principle.

Known from equation (2-7), BLACM is a control object of nonlinearity, and there is coupled action between current component of axis d and current component of axis q. For making BLACM to have same control performance as DC electromotor, it must be decoupled. Rotor field-oriented vector control is a common decoupling control method.

Actually, rotor field-oriented vector control is to put d-q rotating coordinate system at rotor, and it rotating synchronously along with rotor. Its axis d is coincident with the direction of rotor field, axis q is ahead before axis d electrical angle 90 ° at anti-clockwise direction, shown as Figure 2.3. Set $i_d = 0$, equation (2-7) will be simplified as equation (2-9).

$$T_e = p_n \psi_r i_q \tag{2-9}$$

From equation (2-9), the electromagnetic torque can be determined by only torque component current when because and are constant values. This is the main strategy for the field-oriented vector control. By using this

control, the BLACM can be controlled same as DC motors. Figure 2.4 represents block diagram of dual closed-loop vector control system for BLACM.
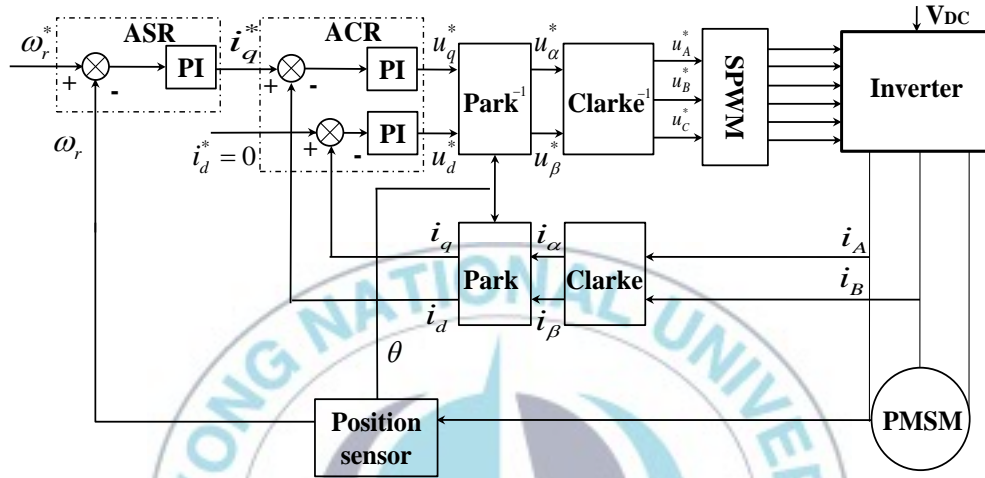
Figure 2.4 The dual closed-loop vector control system for BLACM

2.2.4 Sinusoidal pulse width modulation (SPWM) techniques

Pulse width modulation(PWM)is the key technology in variable frequency speed adjusting system. There are two type common PWM technologies: SPWM technology and SVPWM technology. The control purpose of SPWM is to output sine wave current, while the control purpose of SVPWM is to have the electromotor get ideal round field. These chapters emphatically introduce the technical principle and control method of these two types PWM, and compare their control performance.

2.2.4.1 The principle of SPWM

There is an important conclusion in sampling control theory: when narrow pulses with same impulse (acreage) and different shape impact at

inertia system, their output responds are about the same. Figure 2.5 is several classic narrow pulses with different shape and same acreage. When they impact at a same inertia system, their impact effects are equivalent.
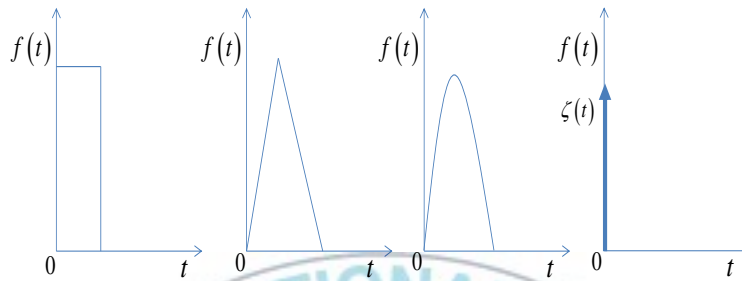
Figure 2.5 The typical narrow pulses of different shapes

According to above principle, any signals with different wave shape are equivalent with series narrow pulses with same acreage. Figure 2.6(a) is the positive half-wave of sinusoidal wave. Equally dividing its abscissa axis k and replace each segment with a rectangle pulse with same acreage. This is the theory basis of SPWM technology. The rectangle pulse in Figure 2.6 (b) is called SPWM modulation pulse.
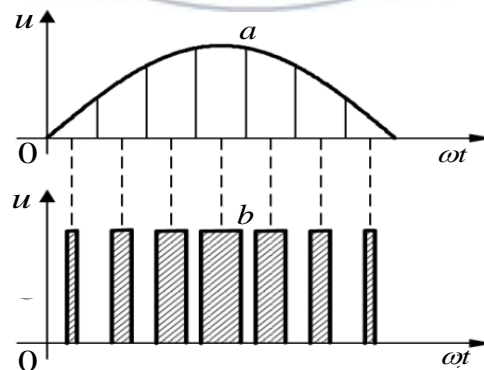
Figure 2.6 PWM waveform generation method

2.2.4.2 Three-phase sinusoidal pulse width modulation

In reality, people confirm the width of SPWM rectangle pulse wave by crossing sinusoidal wave and triangle wave. Shown as Figure 2.7(a), suppose the amplitude of triangle wave v_c is 1, frequency is f_c, the amplitude of A-phase sinusoidal wave $v_{rA} = M \sin \omega t$ is M, frequency is $f_{rA} = \omega/2\pi$, make a rule that when sinusoidal wave is larger than triangle wave, SPWM output high level; in contrary, SPWM output low level. Thus we get a group of rectangle SPWM pulses with same amplitude but different duty ratio (shown as Figure 2.7(b)). Sinusoidal wave v_{rA} is called modulation wave, triangle wave v_c is called carrier wave.
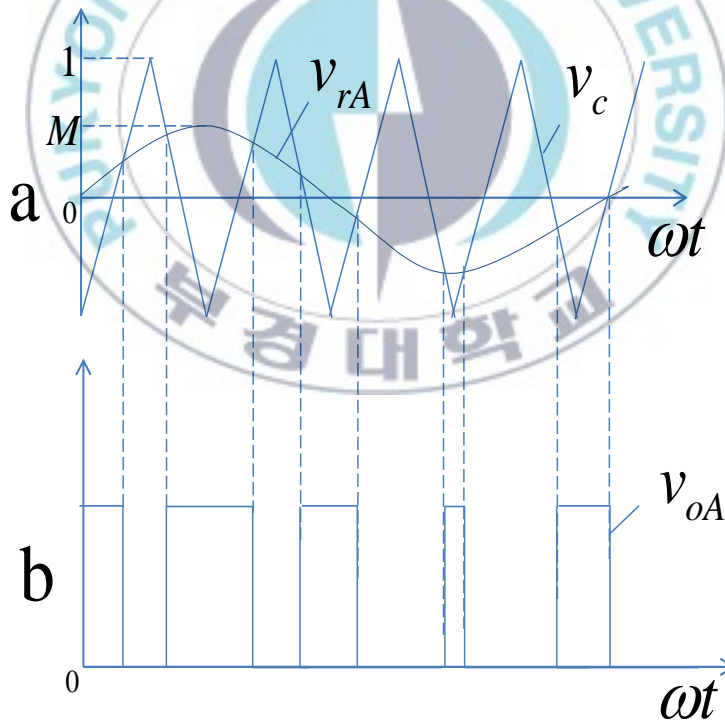
Figure 2.7 SPWM waveform generation method

If pulse width modulation by using 3 phases of symmetrical sinusoidal wave v_{rA}, v_{rB}, v_{rC} which with phase difference 120° as modulation wave and triangle wave v_c as carrier wave, we can get 3 phases of symmetrical SPWM pulses v_{oA}, v_{oB}, v_{oC}. First, running logic negation operation on v_{oA}, v_{oB}, v_{oC} to get $\overline{v_{oA}}, \overline{v_{oB}}$, $\overline{v_{oC}}$. Then we can get 3 phase voltage wave $U_{AN'}$, $U_{BN'}$, $U_{CN'}$ which is of the same shape but different amplitude as v_{oA}, v_{oB}, v_{oC} at output side of inverter by using v_{oA}, v_{oB}, v_{oC} ($\overline{v_{oA}}$, $\overline{v_{oB}}$, $\overline{v_{oC}}$) to control the breakover and close of 3 IGBTs of upper(down) bridge arm in 3 phase inverter, shown as Figure 2.9(a, b, c).
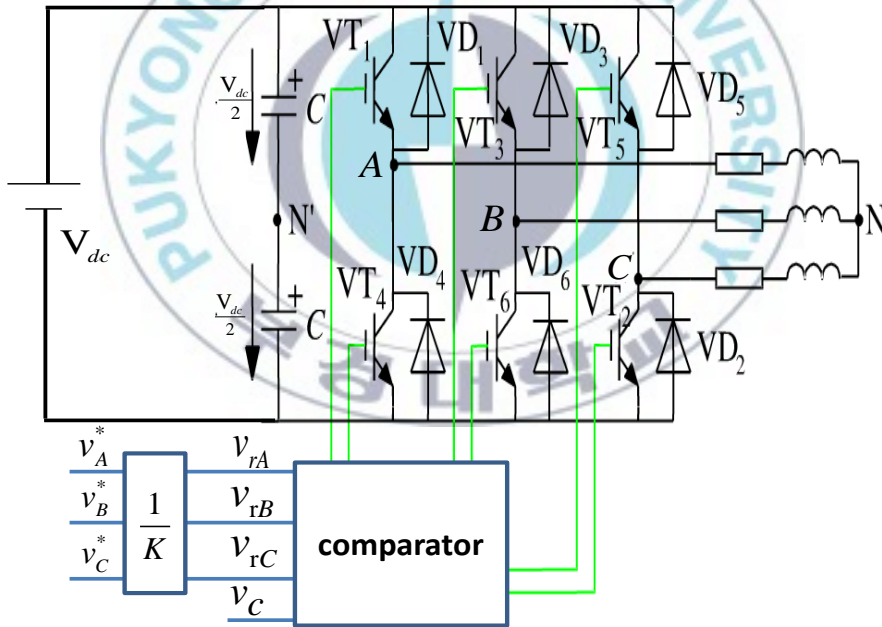
Figure 2.8 The principle diagram of the SPWM inverter
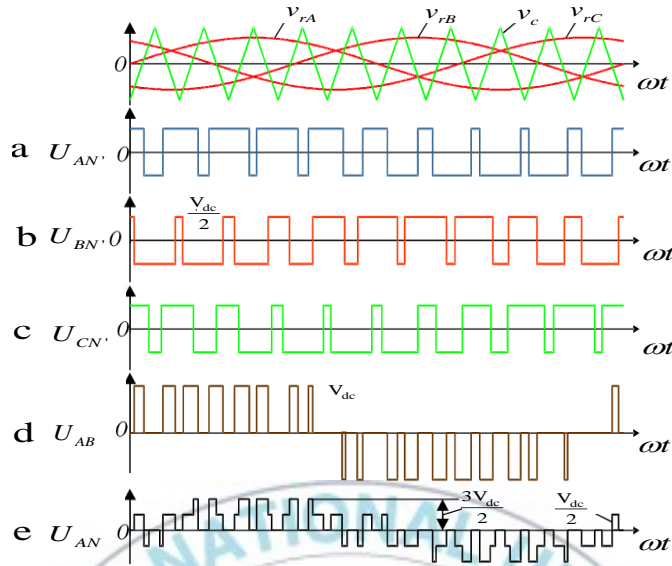
Figure 2.9 The principle diagram of inverter output waveform

The load line voltage U_{AB}, U_{BC}, U_{CA} of inverter could be acquired from equation (2-10). The wave shape of U_{AB} is shown as Figure 2.9(d).

$$\left.\begin{array}{l} U_{AB} = U_{AN'} - U_{BN'} \\ U_{BC} = U_{BN'} - U_{CN'} \\ U_{CA} = U_{CN'} - U_{AN'} \end{array}\right\} \qquad (2\text{-}10)$$

Load phase voltage U_{AN}, U_{BN}, U_{CN} could be acquired from equation (2-11) , equation (2-12) and equation (2-13). The wave shape of U_{AN} is shown as Figure 2.9 (e).

$$\left.\begin{array}{l} U_{AN} = U_{AN'} - U_{NN'} \\ U_{BN} = U_{BN'} - U_{NN'} \\ U_{CN} = U_{CN'} - U_{NN'} \end{array}\right\}$$

$$(2\text{-}11)$$

$$U_{NN'} = \frac{1}{3}(U_{AN'} + U_{BN'} + U_{CN'}) - \frac{1}{3}(U_{AN} + U_{BN} + U_{CN}) \qquad (2\text{-}12)$$

If the loads of 3 phases are completely the same, then $U_{AN} + U_{BN} + U_{CN} = 0$, there is

$$U_{NN'} = \frac{1}{3}(U_{AN'} + U_{BN'} + U_{CN'}) \qquad (2\text{-}13)$$

Expanding output line voltage U_{AB} by using Fourier series, there is:

$$U_{AB} = \frac{2\sqrt{3}V_{dc}}{\pi}\left[\sin\omega t \sum_{n}\frac{1}{n}(-1)^{k}\sin n\omega t\right] \qquad (2\text{-}14)$$

In equation (2-14), $n = 6k \pm 1$, k is natural number.

The amplitude U_{ABm} and effective value U_{AB} of fundamental wave of output line voltage are:

$$U_{ABm} = \frac{\sqrt{3}V_{dc}}{2} = 0.866V_{dc} \qquad (2\text{-}15)$$

$$U_{AB} = \frac{\sqrt{3}V_{dc}}{2\sqrt{2}} = 0.612V_{dc} \qquad (2\text{-}16)$$

As the same, the amplitude U_{AN1m} and effective value U_{AN1} of fundamental wave of output phase voltage are:

$$U_{AN1m} = \frac{2V_{dc}}{\pi} = 0.637V_{dc} \qquad (2\text{-}17)$$

$$U_{AN1} = \frac{U_{AN1m}}{\sqrt{2}} = 0.45 V_{dc} \tag{2-18}$$

2.2.4.3 Symmetrical rules sampling method of SPWM

The real time compute of SPWM signal require corresponding mathematical model. There are several methods to establish mathematical model, for example harmonic elimination, area equalization, sampling SPWM, etc. Sampling SPWM method is also divided into natural sampling, symmetrical rules sampling, unsymmetrical rules sampling, etc. This paper emphatically introduces the symmetrical rules sampling method.
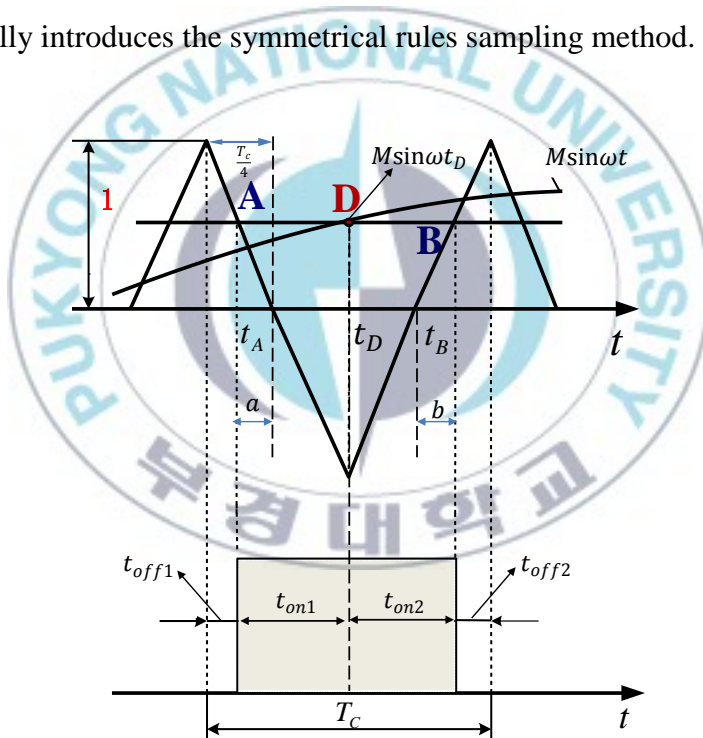
Figure 2.10 The principle diagram of symmetrical rules sampling

Symmetrical rules sampling method regards every time of low symmetry axis of triangle load wave v_c as sampling time, shown as Figure 2.10. Drawing a parallel with t axis which through the cross point D of low

symmetry axis of v_c and modulation wave v_{rA}. Taking the cross point A and B of this parallel and the two sides of triangle wave as "breakover" and "close" time of SPWM, shown as Figure 2.10. T_c is the period of SPWM(period of v_c), t_{on} and t_{off} represent the last time of high level and low level separately, t_D is sampling time.

Here we deduct the mathematical model of symmetrical rules sampling of SPWM, known from $0 \le M \le 1$,

$$\left. \begin{aligned} t_{off1} &= \frac{T_c}{4} - a \\ t_{on1} &= \frac{T_c}{4} + a \\ t_{off2} &= \frac{T_c}{4} - b \\ t_{on2} &= \frac{T_c}{4} + b \end{aligned} \right\} \tag{2-19}$$

According to principle of similarity of triangle:

$$\left. \begin{aligned} \frac{a}{(T_c/4)} &= \frac{M \sin \omega t_D}{1} \\ a &= b \end{aligned} \right\}$$

$$\left. \begin{aligned} a &= \frac{T_c}{4} M \sin \omega t_D \\ b &= \frac{T_c}{4} M \sin \omega t_D \end{aligned} \right\} \tag{2-20}$$

From equation (2-19) and equation (2-20):

18

$$t_{off1} = \frac{T_c}{4}(1 - M \sin \omega t_D)$$
$$t_{on1} = \frac{T_c}{4}(1 + M \sin \omega t_D)$$
$$t_{off2} = \frac{T_c}{4}(1 - M \sin \omega t_D)$$ (2-21)
$$t_{on2} = \frac{T_c}{4}(1 + M \sin \omega t_D)$$

$$t_{on} = t_{on1} + t_{on2} = \frac{T_c}{2}(1 + M \sin \omega t_D)$$ (2-22)

$$\frac{t_{on}}{T_c} = \frac{1}{2}(1 + M \sin \omega t_D)$$ (2-23)

In equation (2-23), t_{on}/T_c is the duty ratio of SPWM rectangle wave pulse. In real systems, we could sampling the value of modulation wave($M \sin \omega t$) with time interval T_c, and compute the duty ratio by equation (2-23), then generating PWM pulse of this duty ratio from processor. If sampling rapidly and continuously, PWM signals which duty ratio continuously changing will happen, the changing period of duty ratio is T_c as well.

M is modulation coefficient($0 \le M \le 1$), it is equal to amplitude of modulation wave v_{rA} divide with amplitude of triangle carrier wave, Because the amplitude of triangle carrier wave v_c is 1, so M is equal to the amplitude of modulation wave v_{rA}.

Though there is minor error in symmetrical rules sampling method of SPWM, it has been widely used in engineering operations for it simplified the compute process greatly.

2.2.5 Space vector pulse width modulation(SVPWM) techniques

SPWM law sampling method is expecting to get a sine wave power supply, in which three phases are symmetrical, while voltage and frequency are adjustable. Its control principle is to reduce the harmonic component of output as far as possible. Though this method has advantages of simple model and easy to realize, it has disadvantage of low usage ratio of voltage.

The most popular and effective method nowadays is voltage Space Vector Pulse Width Modulation(SVPWM) technology. It is also called linkage path method. This method is based on electromotor. Its control purpose is to have AC electromotor generate round rotating field.

2.2.5.1 Voltage space vector and flux vector

Voltage space vector is defined by space position of three phase windings. A plane static coordinate system could be defined by three phase stator windings, shown on Figure 2.11. This special coordinate system use three axises with angle interval 120° to indicate three phase windings. The voltage at three phase windings contribute to voltage space vector u_A, u_B, u_C, their directions always at axises, and size change according to sine law along with time. So the sum of vectors(u) of u_A, u_B, u_C is voltage space vectors which rotate with angular speed ω, and ω is the angular frequency of power supply.
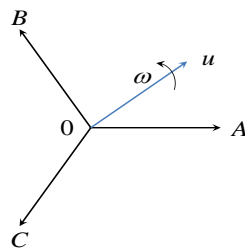
Figure 2.11 A-B-C coordinate system

$$\mathbf{u} = \mathbf{u_A} + \mathbf{u_B} + \mathbf{u_C} \tag{2-24}$$

In the same way, the space vector $\mathbf{I}$ and $\mathbf{\psi}$ of current and linkage could be defined, and their relationship is as below:

$$\mathbf{u} = R\mathbf{I} + \frac{d\mathbf{\psi}}{dt} \tag{2-25}$$

When the rotating speed is not too slow in electromotor, the voltage drop of the resistance R of stator is relatively small, so it could be ignored. Equation (2-25) could be simplified as

$$\mathbf{u} \approx \frac{d\mathbf{\psi}}{dt}$$

$$\mathbf{\psi} \approx \int \mathbf{u} dt \tag{2-26}$$

$$\mathbf{\psi} = \mathbf{\psi}_m e^{j\omega t} \tag{2-27}$$

$$\mathbf{u} = \frac{d(\mathbf{\psi}_m e^{j\omega t})}{dt} = j\omega \mathbf{\psi}_m e^{j\omega t} = \omega \mathbf{\psi}_m e^{j(\omega t + \pi/2)} \tag{2-28}$$

Equation (2-28) shows that, when the amplitude of linkage $\mathbf{\psi}_m$ is constant, the size of $\mathbf{u}$ is in proportion to ω, and the direction of $\mathbf{u}$ is along with the tangent line of the round path of linkage. When the linkage vector rotate one circle in space, the voltage vector also continuously moved 2π radian along with the tangent line of linkage round and its movement path is coincident with linkage round.

2.2.5.2 Basic voltage space vector

Figure 2.12 is a classic voltage-type inverter. The movement path of **u** could become round by adjusting the switch status of IGBT, switch sequence and switch time. Detailed operation is as below.
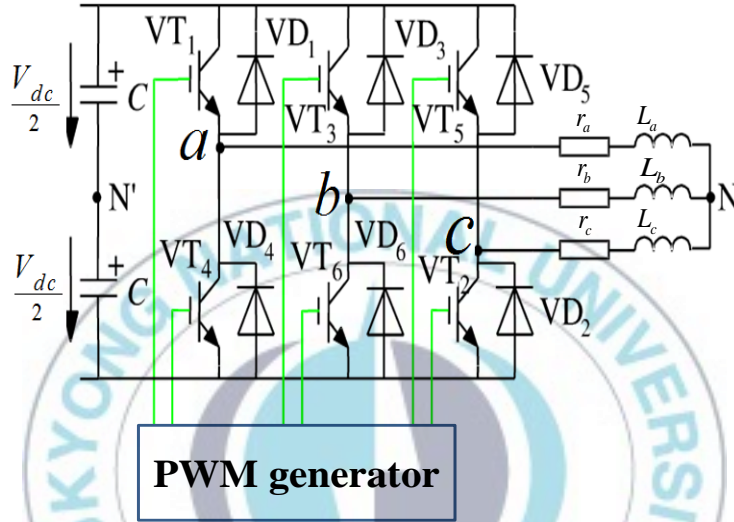
Figure 2.12 The principle diagram of the SVPWM inverter

VT_1-VT_6 in Figure 2.12 indicates 6 IGBT. a, b, c indicate the 3 bridge arms of inverters separately. When the IGBT of upper bridge arm in breakover status (At this time, the IGBT of down bridge arm must close), the switch status of this bridge arm is defined as "1". Otherwise, the switch status is 0. Thus a, b, c forms $8(2^3=8)$ switch modes like 000, 001, 010, 011, 100, 101, 110 and 111. Among them, 000 and 111 are called as zero status, because at that time, there is no voltage output from inverter.

By deduction, the relationship between line voltage vector $[U_{AB} \ U_{BC} \ U_{CD}]^T$ of output of 3 phase inverter and switch status vector $[a \ b \ c]^T$ is:

22

$$\begin{bmatrix} U_{AB} \\ U_{BC} \\ U_{CD} \end{bmatrix} = V_{dc} \begin{bmatrix} 1 & -1 & 0 \\ 0 & 1 & -1 \\ -1 & 0 & 1 \end{bmatrix} \begin{bmatrix} a \\ b \\ c \end{bmatrix}$$

(2-29)

$$U_{AB\text{m}} = V_{dc}$$

The relationship between phase voltage vector $[U_A \ U_B \ U_C]^T$ of output of 3 phase inverter and switch vector $[a \ b \ c]^T$ is:

$$\begin{bmatrix} U_A \\ U_B \\ U_C \end{bmatrix} = \frac{1}{3} V_{dc} \begin{bmatrix} 2 & -1 & -1 \\ -1 & 2 & -1 \\ -1 & -1 & 2 \end{bmatrix} \begin{bmatrix} a \\ b \\ c \end{bmatrix}$$

(2-30)

In the formula, V_{dc} is the bus voltage of DC.

The correspondence relationship between equation (2-29) and equation (2-30) could be shown as Table 2.2.

Table 2.2 The relation of switch state with phase voltage and line voltage

a	b	c	U_A	U_B	U_C	U_{AB}	U_{BC}	U_{CA}
0	0	0	0	0	0	0	0	0
1	0	0	$2V_{dc}/3$	$-V_{dc}/3$	$-V_{dc}/3$	V_{dc}	0	$-V_{dc}$
1	1	0	$V_{dc}/3$	$V_{dc}/3$	$-2V_{dc}/3$	0	V_{dc}	$-V_{dc}$
0	1	0	$-V_{dc}/3$	$2V_{dc}/3$	$-V_{dc}/3$	$-V_{dc}$	V_{dc}	0
0	1	1	$-2V_{dc}/3$	$V_{dc}/3$	$V_{dc}/3$	$-V_{dc}$	0	V_{dc}
0	0	1	$-V_{dc}/3$	$-V_{dc}/3$	$2V_{dc}/3$	0	$-V_{dc}$	V_{dc}
1	0	1	$V_{dc}/3$	$-2V_{dc}/3$	$V_{dc}/3$	V_{dc}	$-V_{dc}$	0
1	1	1	0	0	0	0	0	0

The space vector and phase angle of phase voltage could be solved by substituting the 8 groups of phase voltage in Table 2.1 into equation (2-24). The sums of these 8 vectors are so called basic voltage space vector. According to the feature of their phase angle, they are named as U_{000}, U_0, U_{60}, U_{120}, U_{180}, U_{240}, U_{360}, U_{111} separately. Among them, U_{000}, U_{111} are called as zero vector, other 6 vectors are called non-zero vector. The size and position of the 8 basic voltage space vectors are given in Figure 2.13. Among them, the amplitude of non-zero vector is the same (length is $2V_{dc}/3$), the interval between neighboring vector is $60°$, while the amplitude of the two zero vector is zero and located at the center.

By using Clarke transformation, transforming the phase voltage in 3 phase *A-B-C* plane coordinate system into α-β rectangular plane coordinate system. Its transforming formula is:

$$\begin{bmatrix} U_\alpha \\ U_\beta \end{bmatrix} = \sqrt{\frac{2}{3}} \begin{bmatrix} 1 & -\frac{1}{2} & -\frac{1}{2} \\ 0 & \frac{\sqrt{3}}{2} & -\frac{\sqrt{3}}{2} \end{bmatrix} \begin{bmatrix} U_A \\ U_B \\ U_C \end{bmatrix} \tag{2-31}$$

According to equation (2-31), the corresponding phase voltages in Table 2.1 which are related to switch status a, b, c could be transformed as components in α-β rectangular plane coordinate system. Transforming results are shown as Table 2.3 and Figure 2.13.
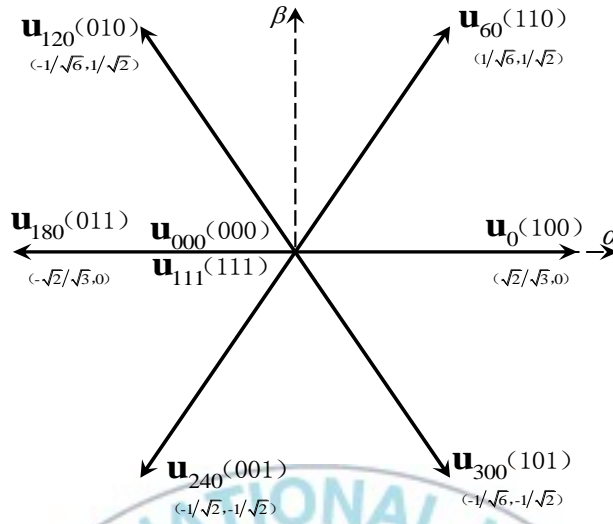
Figure 2.13 The principle diagram basic voltage space vector

2.2.5.3 Flux linkage track control

Shown as Figure 2.14, if the 6 non-zero basic voltage space vector output in turn, then the movement track of the flux linkage vector ψ is a regular hexagon. And this regular hexagon is equally divided into 6 sectors, marked as I, II, III, IV, V and VI.

Obviously, only rotating field of regular hexagon shape could be formed under this power supply method, rather than round rotating field as we expected.

How to acquire round rotating field? If rotating filed is a regular polygon, we could acquire a similar round rotating filed. Obviously, the more sides the regular polygon has, the more similar to round. But there are only 6 non-zero basic voltage space vectors. If we expect the rotating filed has as more sides as possible, there must be more switch status of inverter. We could acquire more switch status by taking the advantage of the linear time combination of 6 non-zero basic voltage space vectors.

Table 2.3 The relation of switch state with U_α and U_β

a	b	c	U_α	U_β	
0	0	0	0	0	$\mathbf{U}_{000}$
1	0	0	$\sqrt{2/3}V_{dc}$	0	$\mathbf{U}_0$
1	1	0	$\sqrt{1/6}V_{dc}$	$\sqrt{1/2}V_{dc}$	$\mathbf{U}_{60}$
0	1	0	$-\sqrt{1/6}V_{dc}$	$\sqrt{1/2}V_{dc}$	$\mathbf{U}_{120}$
0	1	1	$-\sqrt{2/3}V_{dc}$	0	$\mathbf{U}_{180}$
0	0	1	$-\sqrt{1/6}V_{dc}$	$-\sqrt{1/2}V_{dc}$	$\mathbf{U}_{240}$
1	0	1	$\sqrt{1/6}V_{dc}$	$-\sqrt{1/2}V_{dc}$	$\mathbf{U}_{360}$
1	1	1	0	0	$\mathbf{U}_{111}$
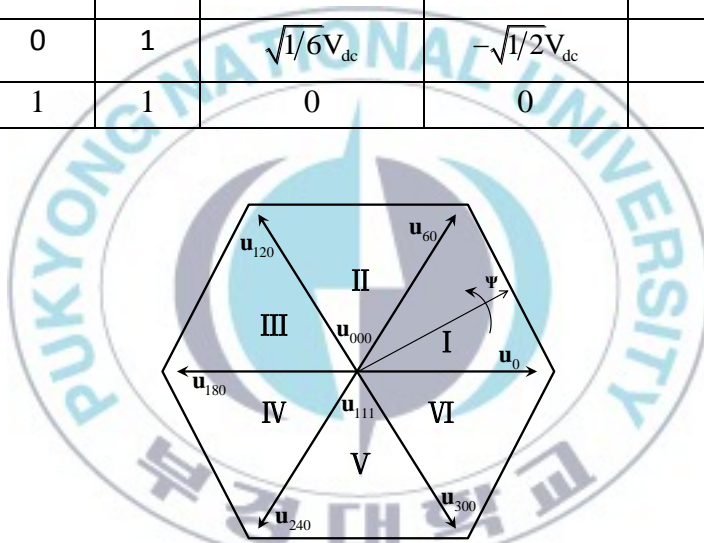
Figure 2.14 The magnetic chain track

The method for linear time combination is introduced as below. In Figure 2.15, $\mathbf{U}_x$ and $\mathbf{U}_{x\pm60}$ are 2 neighboring basic voltage space vector, t_x and $t_{x\pm60}$ are the effective time of $\mathbf{U}_x$ and $\mathbf{U}_{x\pm60}$ separately: $\mathbf{U}_{ref}$ is the reference voltage vector of output. According to the volt-second balance principle in physics, the linear time combination relationship among $\mathbf{U}_{ref}$, $\mathbf{U}_x$ and $\mathbf{U}_{x\pm60}$ is as below:

$$\mathbf{U}_{ref}T_{PWM} = \mathbf{U}_x t_x + \mathbf{U}_{x\pm60} t_{x\pm60} \tag{2-32}$$
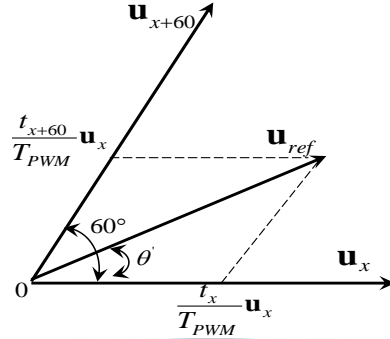
Figure 2.15 The linear combination space vector

According to this method, in next T_{PWM} period, still use the linear time combination of $\mathbf{U}_x$ and $\mathbf{U}_{x\pm60}$, but effective time $t_x^{'}$ and $t_{x\pm60}^{'}$ is different from last time. It must be ensured that the amplitude of new $\mathbf{U}_{ref}^{'}$ of voltage space vector is equal to former $\mathbf{U}_{ref}$.

If it goes on that changing the effective time of neighboring basic vector in every T_{PWM} period, and make sure the combined amplitudes of voltage space vector are equal, enough switch status of inverter could be acquire by this method, so as to make the path of voltage space vector as a regular polygon which is similar to round.

2.2.5.4 Computation for t_x, $t_{x\pm60}$ and t

In Figure 2.15, according to the sine law of triangle, there are:

$$\frac{\mathbf{U}_{ref}}{\sin 120^o} = \frac{\mathbf{U}_x t_x}{T_{PWM}\sin(60^o - \theta^{'})} \tag{2-33}$$

27

$$\frac{\mathbf{U}_{ref}}{\sin 120^{o}} = \frac{\mathbf{U}_{x\pm60}t_{x\pm60}}{T_{PWM}\sin\theta'} \tag{2-34}$$

Known from equation (2-33), (2-34)

$$\left.\begin{array}{l} t_{x} = \dfrac{2\mathbf{U}_{ref}}{\sqrt{3}\mathbf{U}_{x}}T_{PWM}\sin(60^{o}-\theta') \\[4mm] t_{x\pm60} = \dfrac{2\mathbf{U}_{ref}}{\sqrt{3}\mathbf{U}_{x\pm60}}T_{PWM}\sin\theta' \end{array}\right\} \tag{2-35}$$

In Figure 2.14, zero vector $\mathbf{U}_{000}, \mathbf{U}_{111}$ do not output voltage, in another word, they are not effective to electromotor. So in T_{PWM} period, adding zero vectors has no influence to the system. t is the effective time of zero vector $\mathbf{U}_{000}$ or $\mathbf{U}_{111}$.

$$T_{PWM} = t_{x} + t_{x\pm60^{o}} + t \tag{2-36}$$

For making the movement speed of linkage smooth, generally zero vectors are not added intensively, but equally divided into several lots and added into linkage path by several times, while the sum of effective time is still t_{0}, so as to reduce the torque ripple of electromotor.

7 segments SVPWM waves, which are the most popular one, are constituted by 3 segments of zero vectors and 4 segments of non-zero vectors which are neighboring. The 3 zero vectors are located at the start, middle and end of SVPWM wave, shown as Figure 2.16.

See from Figure 2.16, 7 segments SVPWM has features as below:

- Every IGBT only on-off once in every T_{PWM} period, so as to

28

reduce the wastage of switch.

- The 7 segment SVPWM is start and end with zero vector U_{000}, and zero vector U_{111} is in the middle.
- The effective time of zero vector U_{000} and U_{111} are the same. It is $t/2 = (T_{PWM} - t_x - t_{x\pm60^o})/2$.

Sector I

Sector II

SectorIII

SectorIV

Sector V

Sector VI
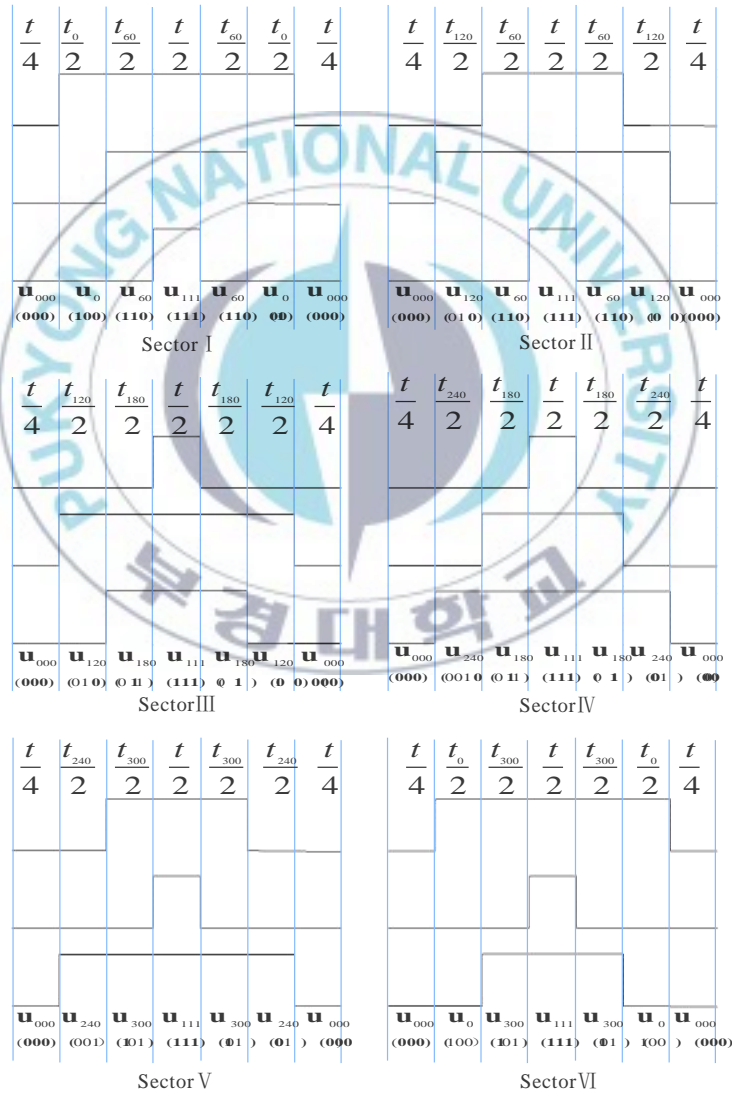
Figure 2.16 The 7 segments SVPWM waves
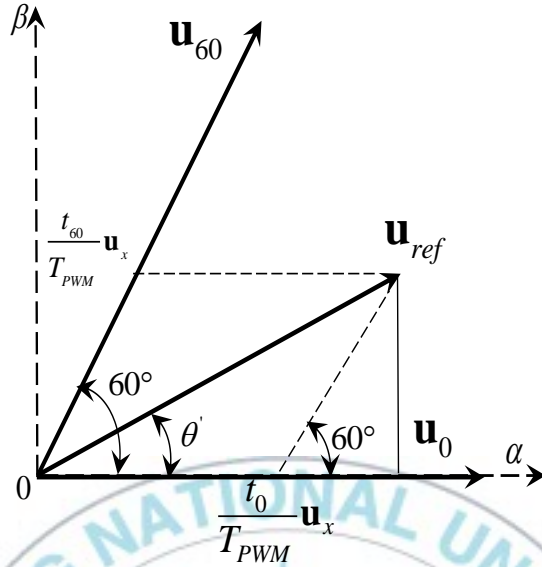
Figure 2.17 The linear combination space vector

In equation (2-32), T_{PWM} is preset according to factors like switch frequency of IGBT, etc. Neighboring basic voltage space vector $\mathbf{U}_x$ and $\mathbf{U}_{x\pm60}$ could be confirmed by judging the sector (it will be introduced hereinafter), but space angle θ' is not easy to acquire. In real system, the influence of θ' could be eliminated only if we fully take the advantage of α-β coordinate system. Analyzing when $\mathbf{U}_{ref}$ at sector I, according to Figure 2.17, there are:

$$\begin{bmatrix} U_\alpha \\ U_\beta \end{bmatrix} T_{PWM} = \left| \mathbf{U}_{ref} \right| T_{PWM} \begin{bmatrix} \cos\theta' \\ \sin\theta' \end{bmatrix} = (\left| \mathbf{U}_0 \right| t_0 + \left| \mathbf{U}_{60} \right| t_{60}) \begin{bmatrix} \cos\theta' \\ \sin\theta' \end{bmatrix}$$

(2-37)

$$= \frac{2}{3} V_{dc} \left\{ \begin{bmatrix} 1 \\ 0 \end{bmatrix} t_0 + \begin{bmatrix} \cos\dfrac{\pi}{3} \\ \sin\dfrac{\pi}{3} \end{bmatrix} t_{60} \right\}$$

Simplifying equation (2-37),

$$
\left.
\begin{aligned}
t_0 &= \frac{\sqrt{3}T_{PWM}}{V_{dc}}\left(\frac{\sqrt{3}U_\alpha}{2} - \frac{U_\beta}{2}\right) \\
t_{60} &= \frac{\sqrt{3}U_\beta T_{PWM}}{V_{dc}} \\
t &= T_{PWM} - t_x - t_{x\pm 60^o}
\end{aligned}
\right\}
\qquad (2\text{-}38)
$$

With the same principle, we can acquire the effective time of two neighboring basic voltage space vector when $\mathbf{U}_{ref}$ in other sectors, shown as Table 2.4.

Table 2.4 Each sector basic space vector duration

Sector	Basic vector duration
I	$t_0 = \dfrac{\sqrt{3}T_{PWM}}{V_{dc}}\left(\dfrac{\sqrt{3}U_\alpha}{2} - \dfrac{U_\beta}{2}\right)$, $\quad t_{60} = \dfrac{\sqrt{3}U_\beta T_{PWM}}{V_{dc}}$
II	$t_{60} = \dfrac{\sqrt{3}T_{PWM}}{V_{dc}}\left(-\dfrac{\sqrt{3}U_\alpha}{2} - \dfrac{U_\beta}{2}\right)$, $\quad t_{120} = \dfrac{\sqrt{3}T_{PWM}}{V_{dc}}\left(\dfrac{\sqrt{3}U_\alpha}{2} - \dfrac{U_\beta}{2}\right)$
III	$t_{120} = \dfrac{\sqrt{3}T_{PWM}}{V_{dc}}U_\beta$, $\quad t_{180} = \dfrac{\sqrt{3}T_{PWM}}{V_{dc}}\left(-\dfrac{\sqrt{3}U_\alpha}{2} - \dfrac{U_\beta}{2}\right)$
IV	$t_{180} = \dfrac{\sqrt{3}T_{PWM}}{V_{dc}}\left(\dfrac{\sqrt{3}U_\alpha}{2} - \dfrac{U_\beta}{2}\right)$, $\quad t_{240} = \dfrac{\sqrt{3}T_{PWM}}{V_{dc}}U_\beta$
V	$t_{240} = \dfrac{\sqrt{3}T_{PWM}}{V_{dc}}\left(-\dfrac{\sqrt{3}U_\alpha}{2} - \dfrac{U_\beta}{2}\right)$, $\quad t_{300} = \dfrac{\sqrt{3}T_{PWM}}{V_{dc}}\left(\dfrac{\sqrt{3}U_\alpha}{2} - \dfrac{U_\beta}{2}\right)$
VI	$t_{300} = \dfrac{\sqrt{3}T_{PWM}}{V_{dc}}U_\beta$, $\quad t_0 = \dfrac{\sqrt{3}T_{PWM}}{V_{dc}}\left(-\dfrac{\sqrt{3}U_\alpha}{2} - \dfrac{U_\beta}{2}\right)$

2.2.5.5 Sectors calculation

Dividing Figure 2.14 into 6 areas which are called sectors, and mark them as I, II, III, IV, V and VI. It's very important to confirm the sector where $\mathbf{U}_{ref}$ at. Because we can only confirm which pair of neighboring basic voltage space vector to be used when we know which sector where $\mathbf{U}_{ref}$ at.

Table 2.5 The necessary and sufficient condition of $\mathbf{U}_{ref}$ in which sector

Sector	The necessary and sufficient condition of $\mathbf{U}_{ref}$ in which sector
I	$U_\alpha > 0$, $U_\beta > 0$ and $U_\alpha/U_\beta < \sqrt{3}$
II	$U_\alpha > 0$ and $U_\beta/|U_\alpha| > \sqrt{3}$
III	$U_\alpha < 0$, $U_\beta > 0$ and $-U_\beta/U_\alpha < \sqrt{3}$
IV	$U_\alpha < 0$, $U_\beta < 0$ and $U_\beta/U_\alpha < \sqrt{3}$
V	$U_\beta < 0$ and $-U_\beta/|U_\alpha| > \sqrt{3}$
VI	$U_\alpha > 0$, $U_\beta < 0$ and $-U_\beta/U_\alpha < \sqrt{3}$

Sector where $\mathbf{U}_{ref}$ could be confirmed by U_α and U_β. Their relationships are shown as below:

Further analyzing above table, and make conclusion as below:

Suppose that B_0, B_1, B_2 have relationship as below:

$$\left. \begin{array}{l} B_0 = U_\beta \\ B_1 = \sin 60^0 U_\alpha - \sin 30^0 U_\beta \\ B_2 = -\sin 60^0 U_\alpha - \sin 30^0 U_\beta \end{array} \right\} \tag{2-39}$$

Compute value of *P* by using equation (2-39)

$$P = 4\operatorname{si} gn(B_2) + 2\operatorname{si} gn(B_1) + \operatorname{si} gn(B_0) \tag{2-40}$$

In Eq(2-40) *sign(B)* is a sign function, its definition is as follow: if *B*>0, then *sign(B)*=1; if *B*<0, then *sign(B)*=0. Then confirming the sector number by checking Table 2.6 according to the value of *P*.

Table 2.6 The sector judgment logic

P	3	1	5	4	6	2
Sector	I	II	III	IV	V	VI

The physical essence of SVPWM is that: SVPWM is a modulation wave which is acquired after added zero-sequence component into three phase sine wave. It's a transformation of SPWM law sampling. But the modulation process of SVPWM is completed in space, while the modulation process of SPWM is completed in A-B-C coordinate system.

2.3 High performance control of BLDCM

Because DC motor has advantages such as easy to control, well mechanical feature, large initial torque, etc, it has been widely used motion control systems. But because of electric brush and inverter, there are several

problems such as spark, noise, etc in DC motor, which influenced the accuracy and performance of speed adjusting of DC motor. Thus a kind of DC motor--brushless DC motor(BLDCM) which without electric brush and inverter come out. BLDCM replaced mechanical commutator and brush with electronic commutator, so this kind of electromotor not only reserved the advantage of DC motor, but also have the advantages of AC motor like simple structure, reliable running, easy for maintenance, etc. Nowadays, BLDCM has been widely used in fields like automobile, electric bicycle, numerical control machine tool, robot, medical equipment, etc.

2.3.1 Basic structure and working principle of BLDCM

At first, this chapter introduced the structure and working principle of brushless electromotor.

2.3.1.1 Basic structure of BLDCM

Basic structure of BLDCM is shown as Figure 2.18. The structure of BLDCM is similar with BLACM. The rotor of BLDCM is also constituted with permanent magnet. There are 2 types BLDCM: surface BLDCM and interior BLDCM. But for acquiring the trapezoidal wave of back emf, the shape of rotor magnets of BLDCM must be camber (tile-shape).
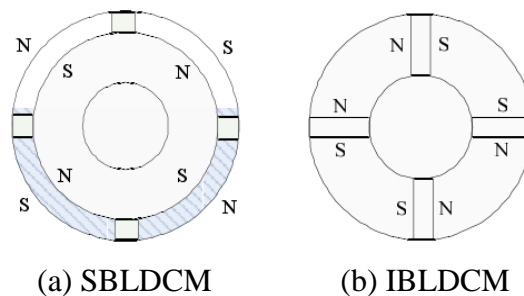

(a) SBLDCM   (b) IBLDCM

Figure 2.18 Sectional drawing of two types of BLDCM

The armature of DC motor is at the rotor, while the stator is static to generate motionless field. For having DC electromotor rotation, the current direction of armature must be continuously changed by using inverter and electric brush, as as to keep two filed directions perpendicular with each other all the time. Thus constant torque will be generated to drive electromotor rotating continuously.

For removing brush, BLDCM put armature at stator, and making rotor with permanent magnet. This structure is just contrary with DC motor. It can always keep the space angle between stator field and rotor permanent magnetic field at 90 °, so as to generate torque to drive motor.

2.3.1.2 Principle and feature of BLDCM

BLDCM control system is mainly constituted with main part of motor, position sensor of rotor, and phase-shifting circuit constituted with controller and inverter. The whole structure of BLDCM control system is shown as Figure 2.19.

Here the basic working principle of BLDCM is explained by taking working method of three-phase six-status as example. Its control circuit is as Figure 2.20, running principle as Figure 2.21.
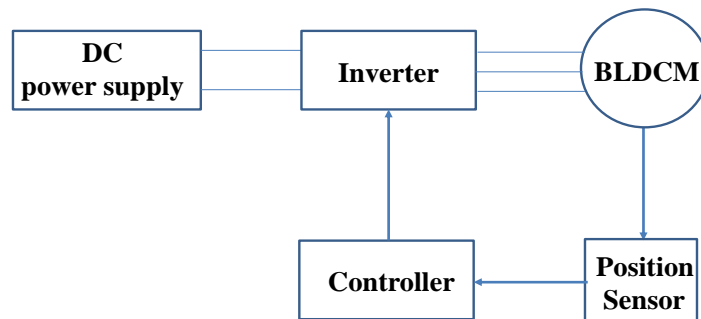

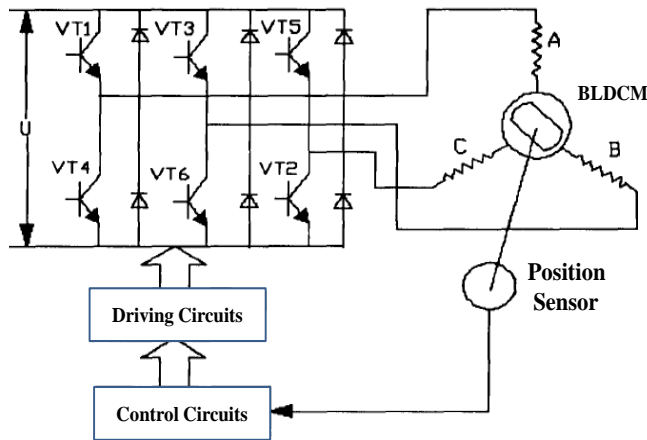Figure 2.19 The diagram of BLDCM control principle

Figure 2.20 The diagram of BLDCM control circuit

To deducting the status of 2 fields as below. Other situations can be deducted by the same way.

(I) When rotor rotating at position shown in Figure 2.21(a), position sensor will output according position information, and control VT_6 and VT_1 to breakover (refer to Figure 2.20). At that time, there are two-phase windings A and B breakover. The direction of current is: positive pole of power supply $\rightarrow VT_1 \rightarrow$ A phase $\rightarrow$ B phase$\rightarrow VT_6 \rightarrow$ positive pole of power supply. Windings of armature will generate magnetic motive force F_a, which will interact with field of rotor to drive electromotor rotating clockwise.

(II) When rotor rotating at 60°electrical angle, shown as Figure 2.21(b), position sensor will output according position information, and control VT_6 and VT_2 to shift phase, that is to make VT_1 and VT_2 breakover. A and C phase power on. The direction of current is: positive pole of power supply $\rightarrow VT_1 \rightarrow$ A phase $\rightarrow$ C phase $\rightarrow VT_2 \rightarrow$ positive pole of power supply. The magnetic motive force generated at that time is shown as Figure 2.21(b). Thus it makes the electromotor to rotate

clockwise. Other situations can be deducted by the same way. Every time, the phase of rotor will change when rotated $60°$ electrical angle, and one of the power tubes will change its phase as well. Every power switching element breakover $120°$ electrical angle. The logic of shifting phase and breakover is VT_6, $VT_1 \rightarrow VT_1$, $VT_2 \rightarrow VT_2$, $VT_3 \rightarrow VT_3$, $VT_4 \rightarrow VT_4$, $VT_5 \rightarrow VT_5$, $VT_6 \rightarrow VT_6$, VT_1. This breakover order will ensure the rotor always to be effected by torque of electromagnetism and continuously rotating clockwise.
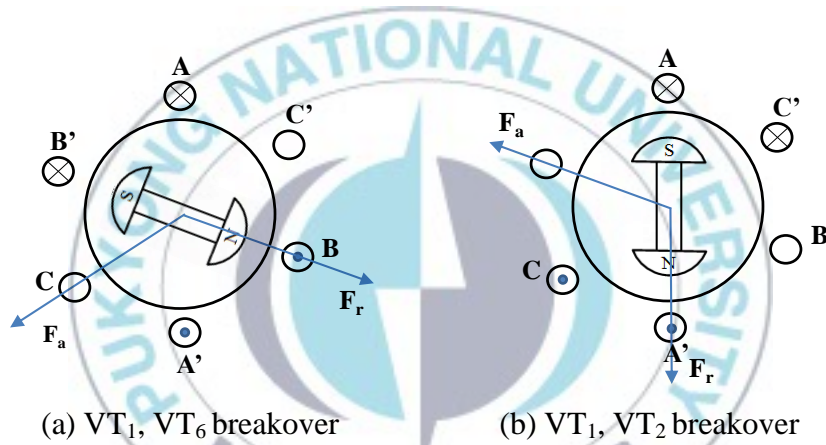

(a) VT_1, VT_6 breakover   (b) VT_1, VT_2 breakover

Figure 2.21 The diagram of BLDCM working principle

2.3.1.3 Mathematical model of BLDCM

Suppose that three-phase winding is complete symmetrical, magnetic circuit is unsaturated, and do not take vortex and magnetic hysteresis loss into consideration, then the equation of three-phase voltage could be shown as:

$$
\begin{bmatrix} u_a \\ u_b \\ u_c \end{bmatrix} = \begin{bmatrix} r & 0 & 0 \\ 0 & r & 0 \\ 0 & 0 & r \end{bmatrix} \begin{bmatrix} i_a \\ i_b \\ i_c \end{bmatrix} + \begin{bmatrix} L & M & M \\ M & L & M \\ M & M & L \end{bmatrix} p \begin{bmatrix} i_a \\ i_b \\ i_c \end{bmatrix} + \begin{bmatrix} e_a \\ e_b \\ e_c \end{bmatrix}
\tag{2-41}
$$

u_a, u_b, u_c : Phase voltage

i_a, i_b, i_c : Phase current

e_a, e_b, e_c : Back emf

L : Self-inductance of winding (H)

M : Mutual inductance of winding (H)

P : Differential operator ($p = d/dt$)

Among them, the electromotive force of square wave and trapezoidal wave of A phase is shown as Figure 2.22.
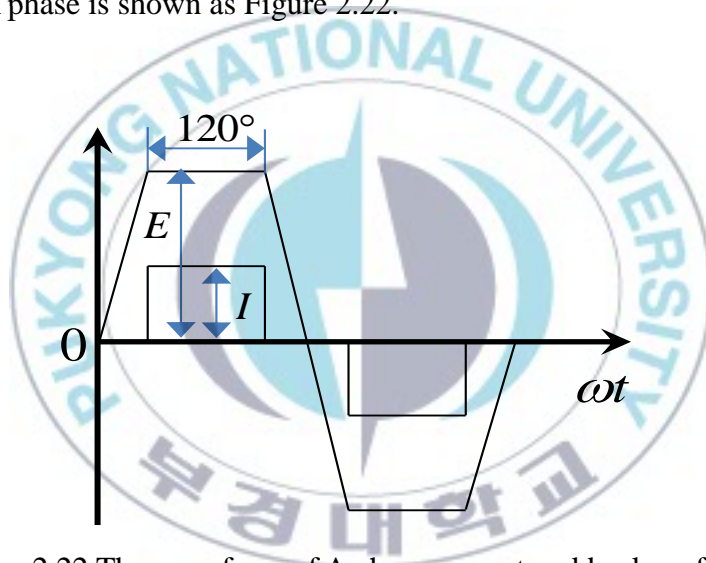

Figure 2.22 The waveform of A phase current and back emf wave

Because, The connection type of three-phase winding is star connection，So

$$i_a + i_b + i_c = 0 \tag{2-42}$$

$$M\,i_a + M\,i_b + M\,i_c = 0 \tag{2-43}$$

So equation (2-41) can be simplified as [4]:

$$\begin{bmatrix} u_a \\ u_b \\ u_c \end{bmatrix} = \begin{bmatrix} r & 0 & 0 \\ 0 & r & 0 \\ 0 & 0 & r \end{bmatrix} \begin{bmatrix} i_a \\ i_b \\ i_c \end{bmatrix} + \begin{bmatrix} L-M & 0 & 0 \\ 0 & L-M & 0 \\ 0 & 0 & L-M \end{bmatrix} p \begin{bmatrix} i_a \\ i_b \\ i_c \end{bmatrix} + \begin{bmatrix} e_a \\ e_b \\ e_c \end{bmatrix} \qquad (2\text{-}44)$$

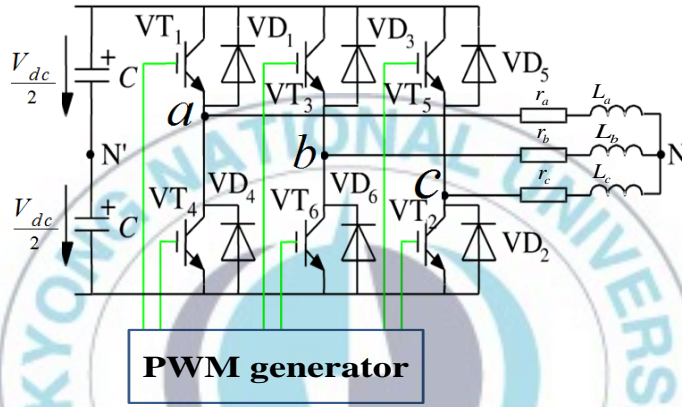Based on this mathematical model of the equivalent circuit for BLDCM as follows[9]:

Figure 2.23 The equivalent circuit for BLDCM

The formula of electromagnetic torque [9]:

$$T_e = \frac{e_a i_a + e_b i_b + e_c i_c}{\omega} \qquad (2\text{-}45)$$

ω is the machinery angular velocity(rad/s) of motor.

From equation (2-45), the value of electromagnetic torque is in a direct ratio with the phase current, so the torque of BLDCM could be controlled by adjusting the amplitude of square current of inverter. For generating constant electromagnetic torque, it requires that the current of stator must be square wave, back emf must be trapezoidal wave. While within every half

cycle, the last time for square wave is $120°$, for flat-topped part of trapezoidal wave of back emf is $120°$, those two should sync completely.

Because BLDCM always has two phase breakover other phase disconnect at any time, so the equation (2-45) can be transform into:

$$T_e = \frac{e_a i_a + e_b i_b + e_c i_c}{\omega} = \frac{2e_m i_m}{\omega} \qquad (2\text{-}46)$$

The motion equations of BLDCM:

$$T_e - T_L - B\omega = J\frac{d\omega}{dt} \qquad (2\text{-}47)$$

T_e : Phase voltage

T_L : Phase current

B : Back emf

J : Self-inductance of winding

This chapter at first analyzed the basic structure and working principle of brushless DC electromotor. Then based on that, analyzed and deducted the mathematical model of BLDCM by taking two-phase breakover star like three-phase six-status BLDCM as example.

2.3.2 A study about reduction BLDCM torque ripple
2.3.2.1 Definition of torque ripple and reasons

Because BLDCM has advantages like easy to control, well mechanical feature, large initial torque, etc, it has been widely used motion control systems. But because of the inherent problem of torque ripple in BLDCM, it

is application in high accuracy and high stable field has been limited badly. So to resolve torque ripple problem of BLDCM is a hotspot in current studies.

The definition of torque ripple is that it is the ratio between the difference between maximum and minimum electromagnetic torque and average electromagnetic torque when running in rated condition [6]:

$$T_r = \frac{T_{max} - T_{min}}{T_N} \times 100\% \tag{2-48}$$

T_r : Torque ripple

T_{max} : Maximum electromagnetic torque

T_{min} : Minimum electromagnetic torque

T_N : Average electromagnetic torque

The main reason of torque ripple is because there is difference between main body of electromotor and its control system. Reference[13] and reference[16] introduced the types of torque ripple in details. Torque ripples are divided into below types:

- Torque ripple caused by grooves: Because there is stator grooves, the reluctance of stator will change along with the changing of rotating angle of rotor. Thus to cause torque ripple.

- Torque ripple caused by armature reaction: The exist of Armature reaction will cause the aberration of air-gap filed of permanent magnet. Thus to cause torque ripple.

- Torque ripple caused by machining: Machining and inconformity of material is another important reason for causing torque ripple.

Torque ripple will be caused by defaults in process error like friction torque unequal, electric parameters of each phase of windings unsymmetrical, performance of each permanent magnet inconformity, etc.

● Torque ripple caused by commutation of current: In every commutation moment in BLDCM, because of the exist of inductance of stator winding, the phase current can not change suddenly, so the current is not the ideal square wave current. Thus to cause torque ripple.

Among them, commutation of current is the main reason for causing torque ripple in BLDCM.

For BLDCM of 2 phase breakover star-shape 3 phase 6 status, there are two phase breakover at any time. Figure 2.24 is the back emf and current wave of BLDCM in ideal status.
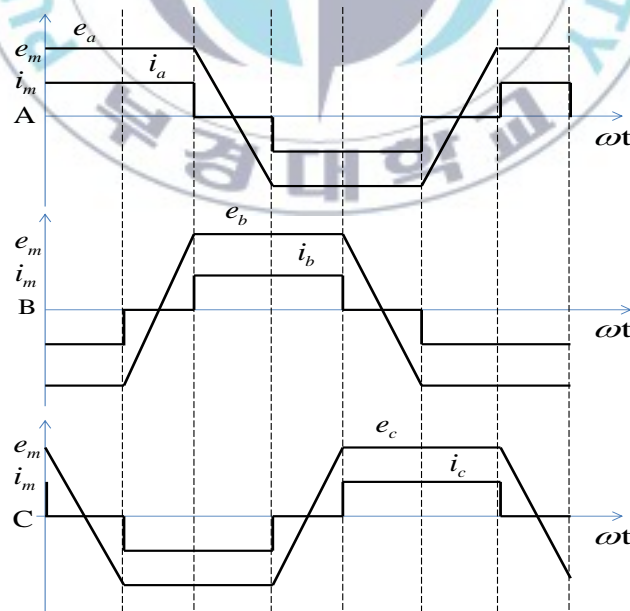

Figure 2.24 The emf waveform and current waveform of ideal state

Known from equation (2-46), electromagnetic torque is:

$$T_e = \frac{2e_m i_m}{\omega} \qquad\qquad (2\text{-}49)$$

e_m : The amplitude of trapezoidal back emf

i_m : The amplitude of phase current

Suppose the main body of electromotor is under ideal status, then e_m is constant. Known from equation (2-49), electromagnetic torque T_e is in proportion to phase current i_m. If current is ideal square current as Figure 2.24 shown, then electromagnetic torque ripple is zero. But in real system, because of the exist of inductance of stator winding, the phase current can not change suddenly, so the current is not the ideal square wave current, but a phase current wave with two peaks shown as Figure 2.25. Known from equation (2-49), torque ripple will certainly increase if phase current i_m has peak.

2.3.2.2 Reduction for BLDCM torque ripple

Known from above analysis, the main reason for torque ripple is the aberration of phase current wave when transforming phase in BLDCM. So only if keep the phase current wave similar with square wave, the torque ripple could be well reduced. For achieving this purpose, we can use strategy of current hysteresis band pulse width modulation(CHBPWM) to directly control BLDCM phase current.
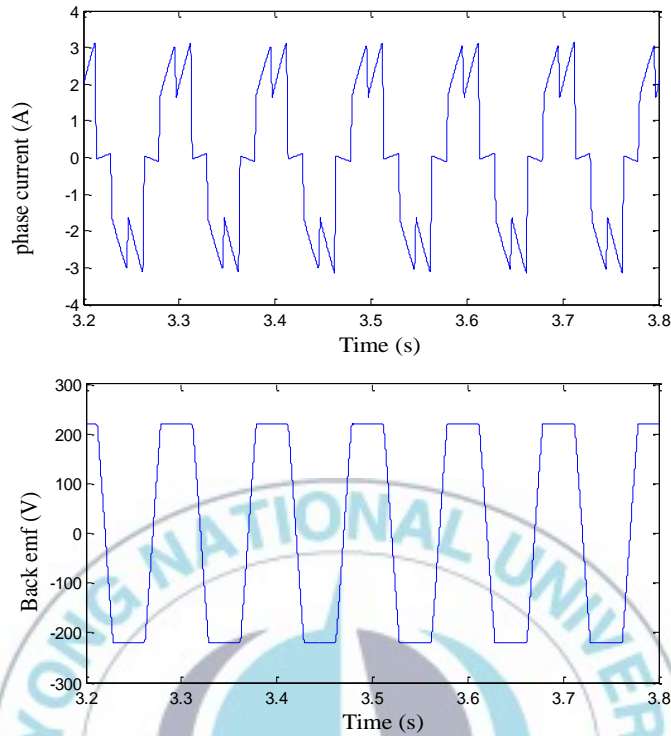
Figure 2.25 Phase current waveform distortion caused by the inductance

2.3.2.3 Basic principle of CHBPWM

The basic principle of CHBPWM is that in current feedback-loop, using current hysteresis controller to compare the size of reference current and feedback current, so as to generate PWM trigger signal. CHBPWM is a thought based on feedback control that to have actual phase current follow the reference current to fluctuate in a small range, shown as Figure 2.27.

Figure 2.26 is the control block diagram of CHBPWM. The working principle of CHBPWM is: when the absolute value of the difference between reference current(i_a^*) and feedback current(i_a) is larger than width of hysteresis(h), the switch tube VT_1 of inverter breakover, switch tube VT_4 off, electromotor connect the positive side of DC bus, the current start to rise. In contrary, the current start to reduce. Selecting proper width of

44

hysteresis could have the actual current continuously follow the wave of reference current, so as to realize the stable control of current.
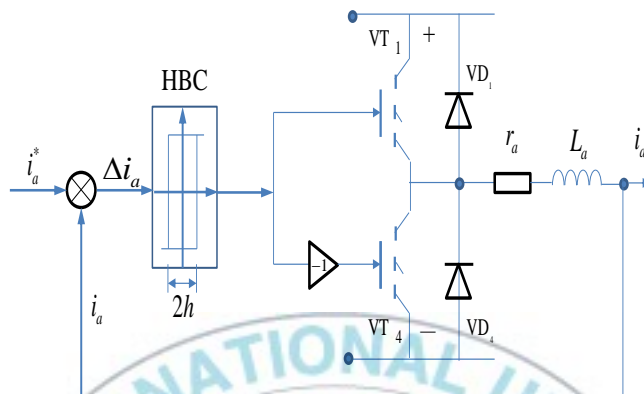

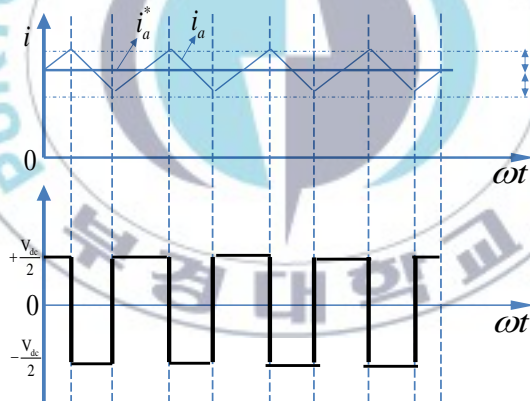
Figure 2.26 The block diagram of CHBPWM control

Figure 2.27 The principle diagram of CHBPWM

Chapter 3

Simulation for BLACM and BLDCM control

3.1 Simulation design for high performance control of BLACM

3.1.1 Simulation model of BLACM

By analyzing mathematical model of BLACM and principle of vector control in last chapter, simulation model of high performance variable frequency speed-adjusting system has been designed based on SPWM and SVPWM with MATIAB/SIMULINK. Design methods for simulation model of BLACM and models of every function module are introduced as below.

The simulation model of main body of BLACM could be called from SIMULINK module database (shown as Figure 3.2.). For different BLACM, related parameters need to be set, for example the number of rotor pole pairs, windings of stator, linkage, etc. Operation is shown as Figure 3.1.

3.1.2 Simulation model of space vector transforming

M language applied with MATLAB transformed formula of space vector transforming equation (2-1), equation (2-2), equation (2-3), equation (2-4) to M program shown as Figure 3.3. Then using module of User-Defined functions in SIMULINK to pack M program as module shown in Figure 3.4.
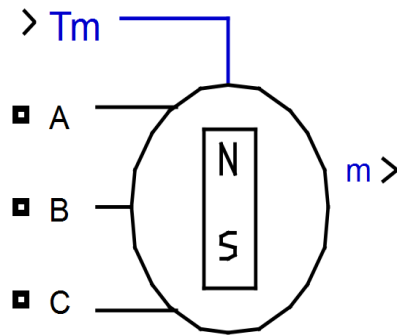
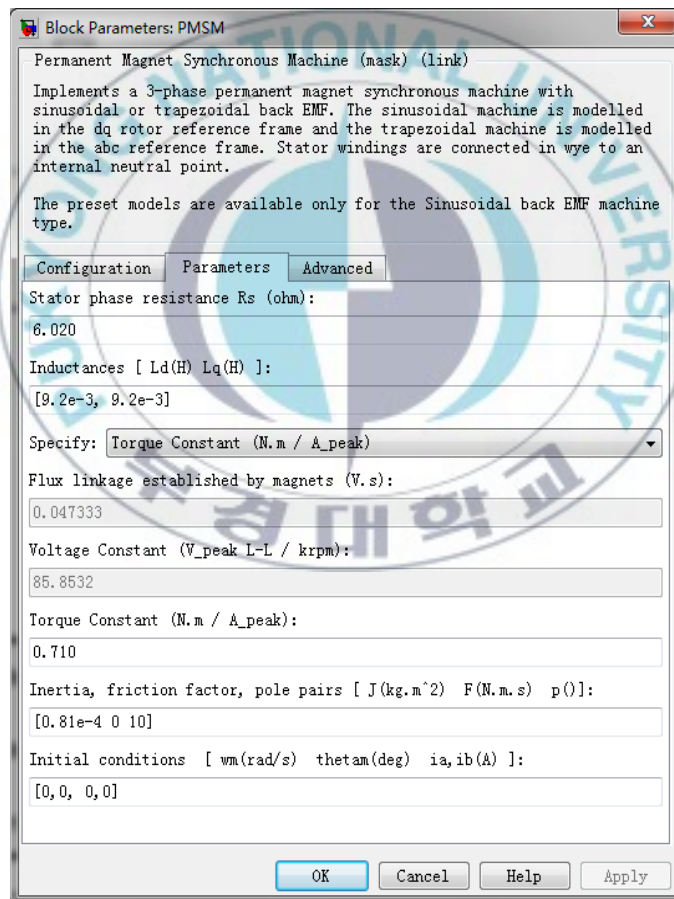Figure 3.1 The block diagram of simulation model for BLACM

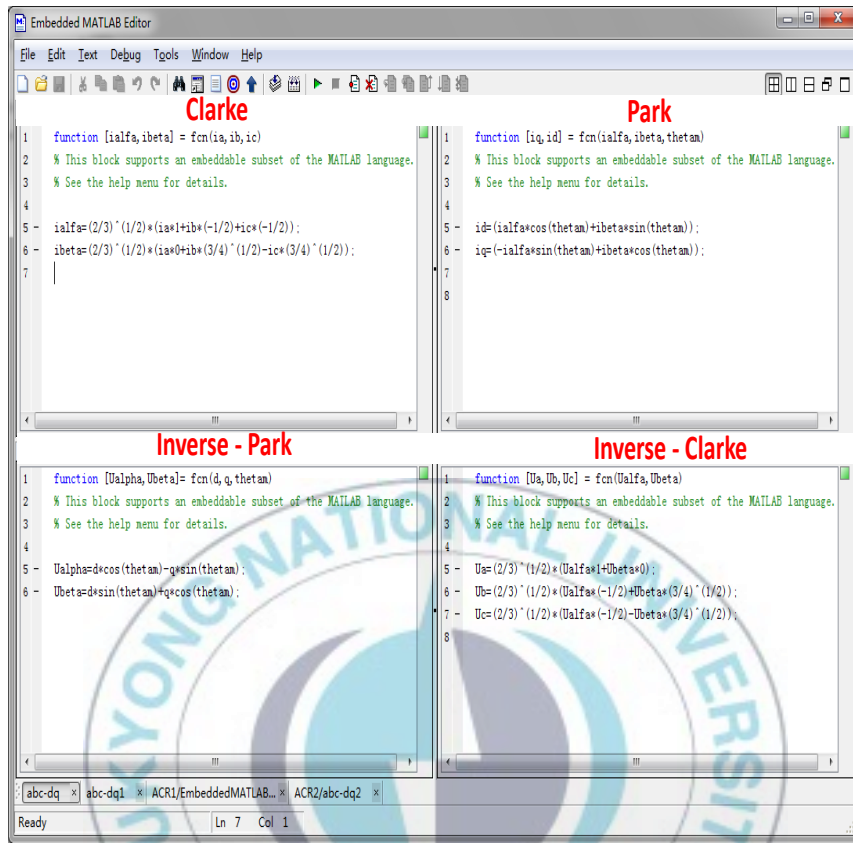Figure 3.2 The parameters set interface of the BLACM model
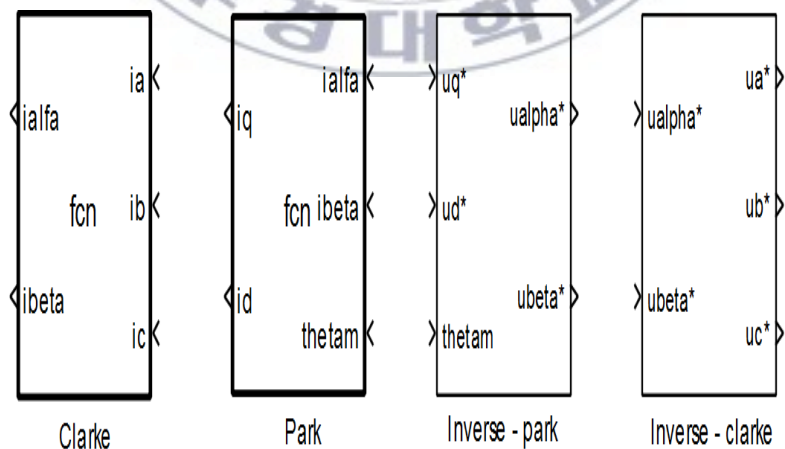
Figure 3.3 M program of vector transform

Figure 3.4 The block diagram of vector transform module

48

3.1.3 Module of variable frequency power supply

Module of variable frequency power supply in BLACM control system is divided into 3 parts: PWM generator, DC voltage source and inverter. Among them, SPWM generator, DC voltage and inverter could be applied with modules in SIMULINK directly. Shown as Figure 3.5.
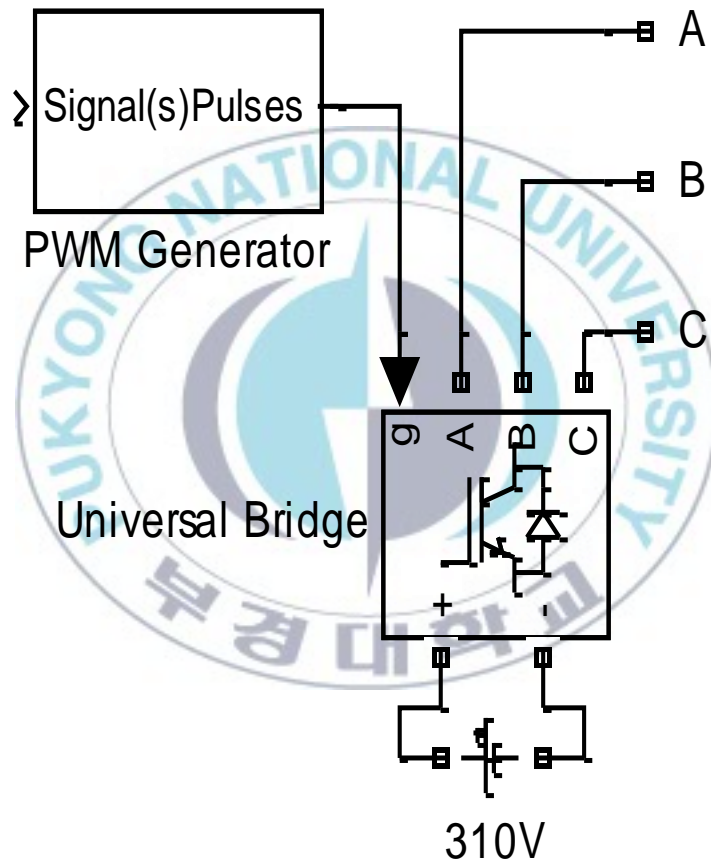

Figure 3.5 The block diagram of power supply module

There is no SVPWM generator module in toolbox of SIMULINK. But we can establish SVPWM generator module shown as Figure 3.6 by applying the principle of SVPWM introduced in chapter 2.
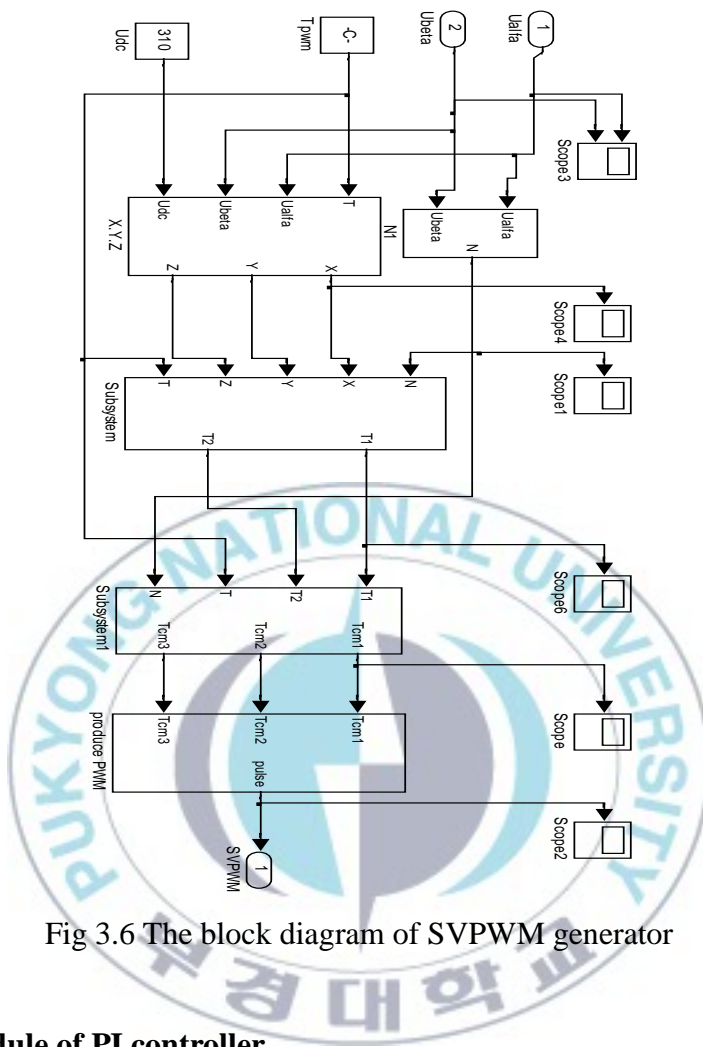
Fig 3.6 The block diagram of SVPWM generator

3.1.4 Module of PI controller

Directly applied with PI controller module in SIMULINK shown as Figure 3.7. This module provided settings for related parameters.
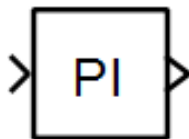

Figure 3.7 The block diagram of PI controller module

3.1.5 Simulation result and analysis of vector control for BLACM

Simulation modules established above have contributed to dual close loop vector control simulation system of BLACM shown as Figure 3.8 and Figure 3.9. Figure 3.8 is applied with SPWM technology, Figure 3.9 is applied with SVPWM technology.

Before simulation, first, set the parameters of BLACM, nominal load $T_L = 2Nm$, reference speed $\omega_e^* = 200\ rad/s$. At first, no load, add nominal load when $t = 1s$. Simulation results are shown as Figure 3.10 and Figure 3.11.

Figure 3.10 and Figure 3.11 show the results of the BLACM control with dual closed-loop vector control algorithm. This dual closed-loop vector control system enhances the control performance of BLACM. The control effect even can be comparable with DC motor control performance. Thus, the dual closed-loop vector control algorithm has been widely used in high-performance speed control systems of BLACM.
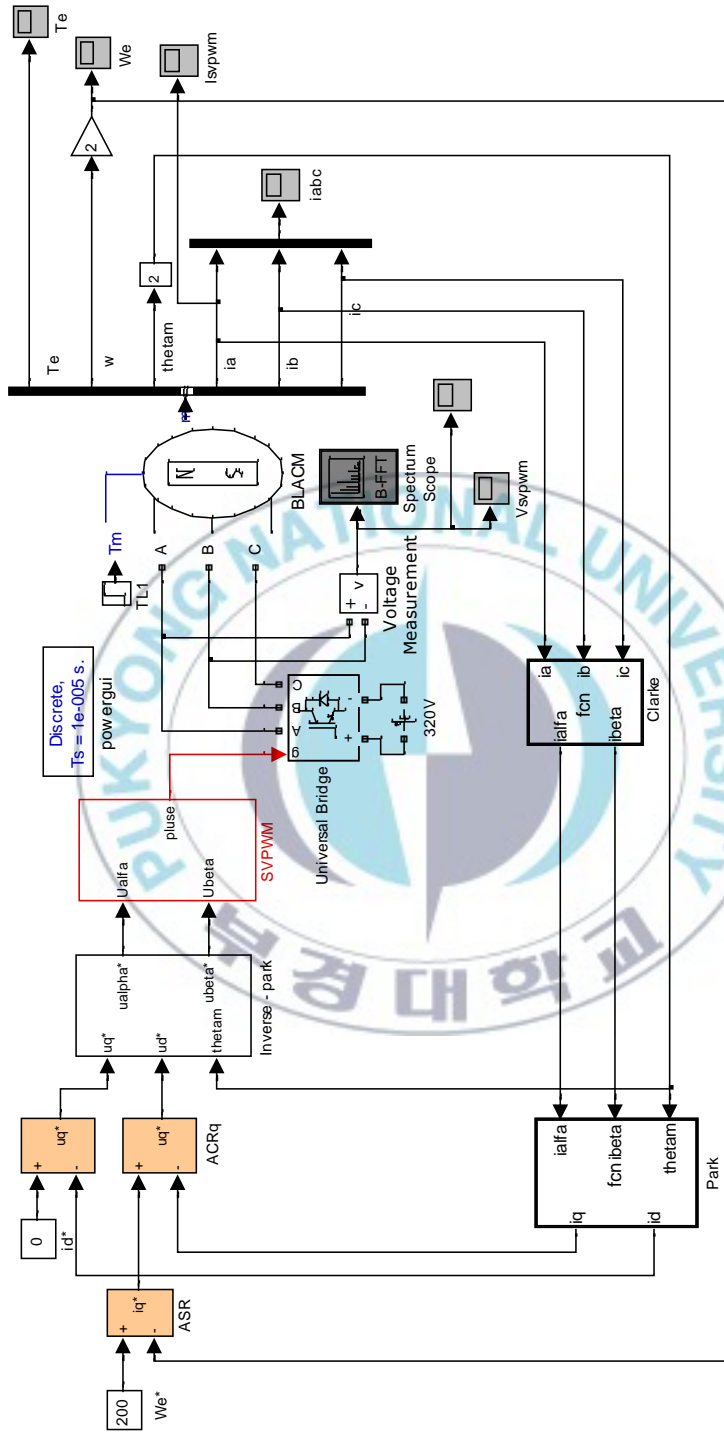
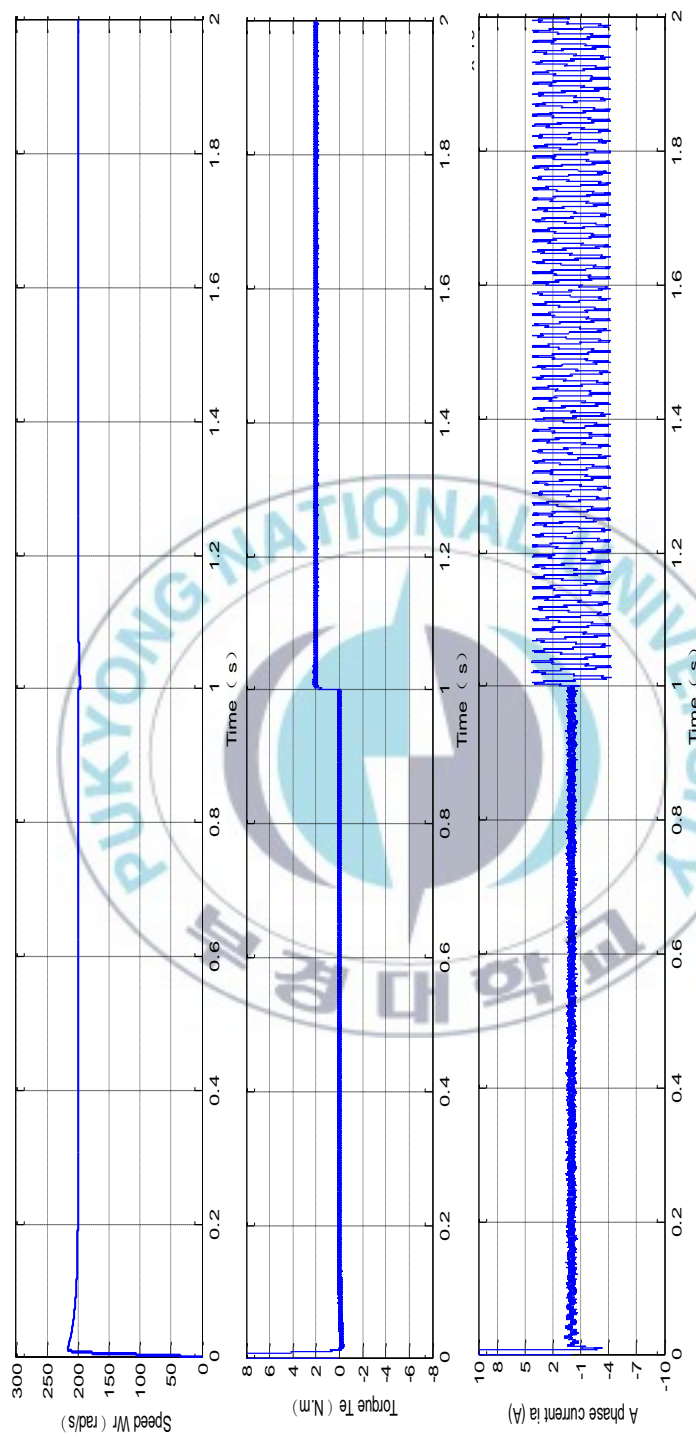Figure 3.8 The block diagram of simulation system for BLACM vector control (SPWM)

Figure 3.9 The block diagram of simulation system for BLACM vector control (SVPWM)

53
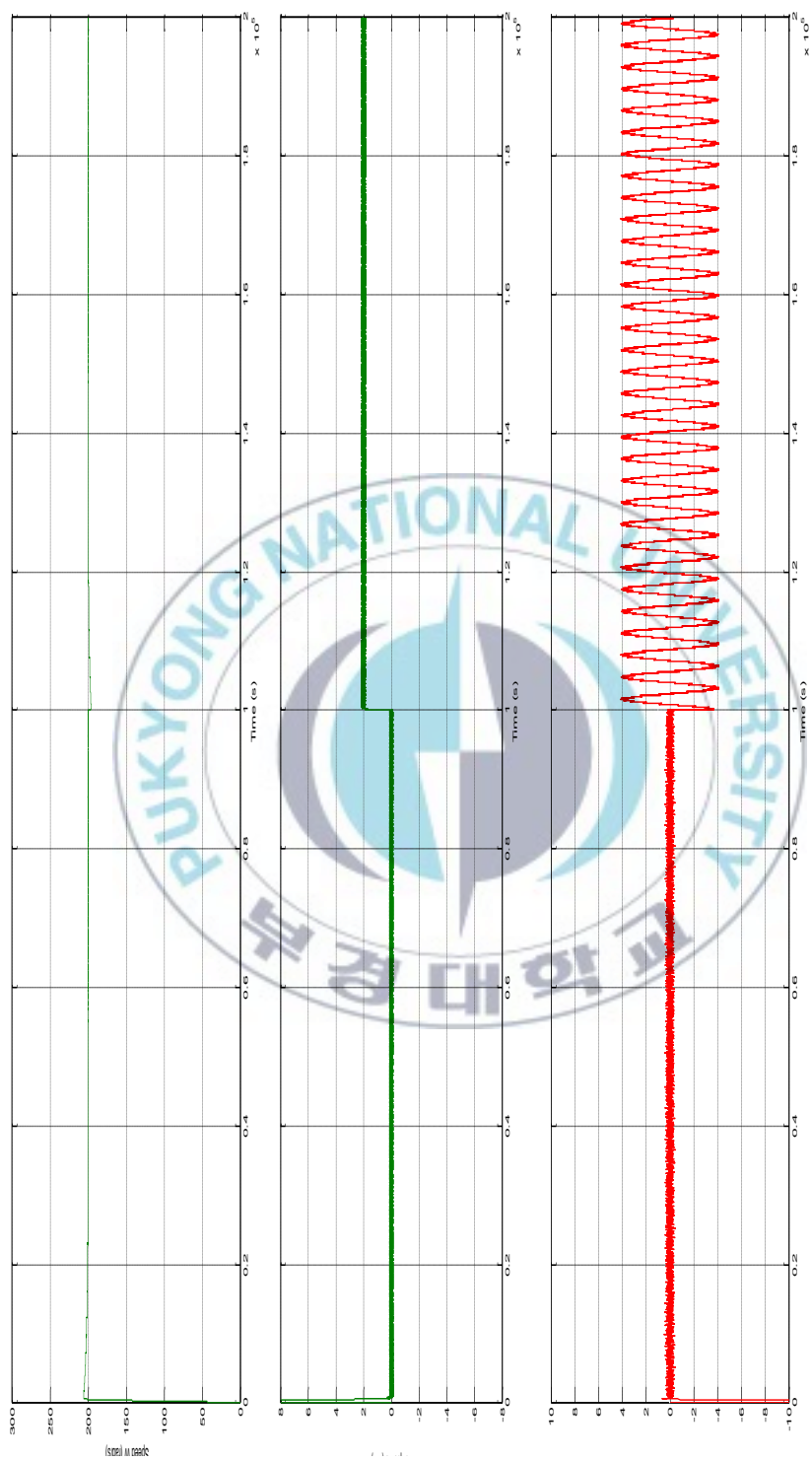
Figure 3.10 The simulation results for SPWM

54

Figure 3.11 The simulation results of speed, torque, phase current for SVPWM

From Figure 3.10 and Figure 3.11, the simulation results are similar, and can not determine what kind of PWM performance is superior, so made the following simulation to compare the performance of SPWM and SVPWM.
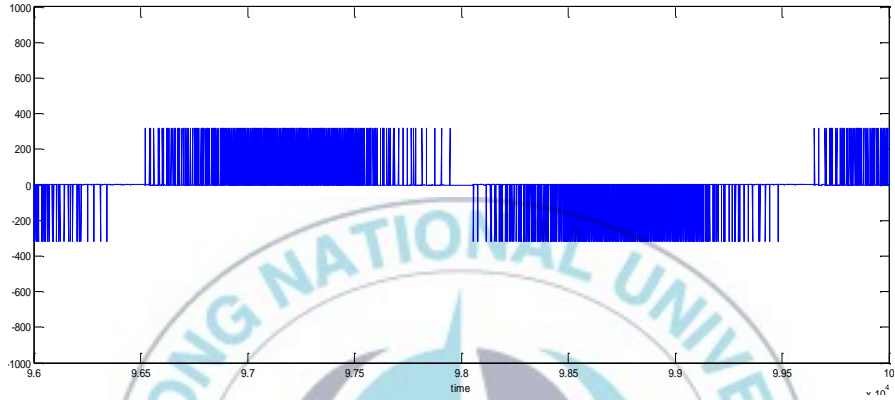

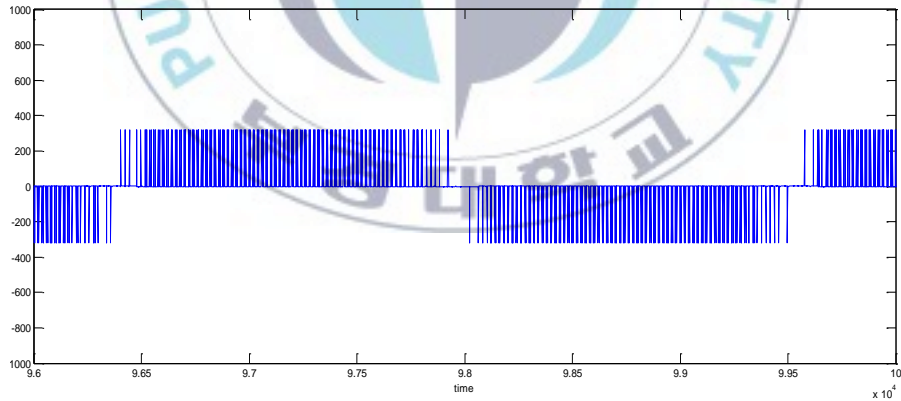Figure 3.12 The simulation results of line voltage U_{AB} for SPWM

Figure 3.13 The simulation results of line voltage U_{AB} for SVPWM

Figure 3.12 and Figure 3.13 are the Simulation results of line voltage U_{AB} for SPWM and SVPWM. By analyzing the density of line voltage waveform can determine the level of the IGBT switch device loss. The more

frequents witching, the shorter life expectancy of IGBT.SVPWM line voltage waveform is less dense; then, switching loss is smaller than SPWM.

Figure 3.14 and Figure 3.15 are the phase current i_{AB} harmonic analysis using FFT(Fast Fourier Transform Algorithm) for SPWM and SVPWM. If THD(Total Harmonic Distortion) is larger, the phase current will have more harmonics. Because of the SVPWM THD=3.61 is smaller than SPWM, so SVPWM has better harmonic suppression effect.
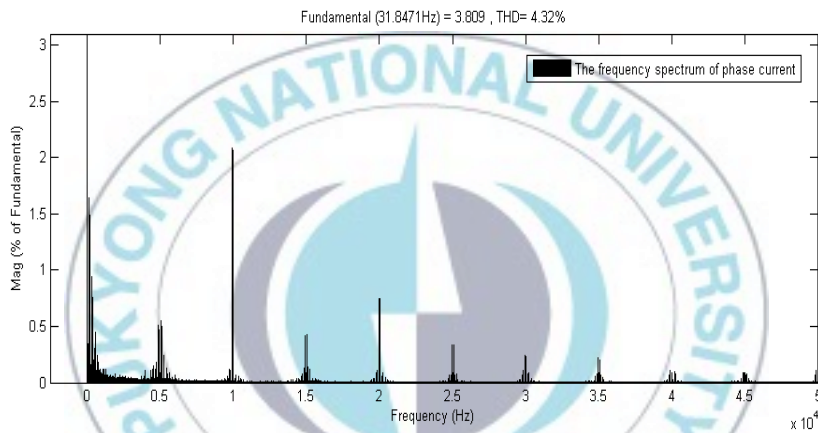

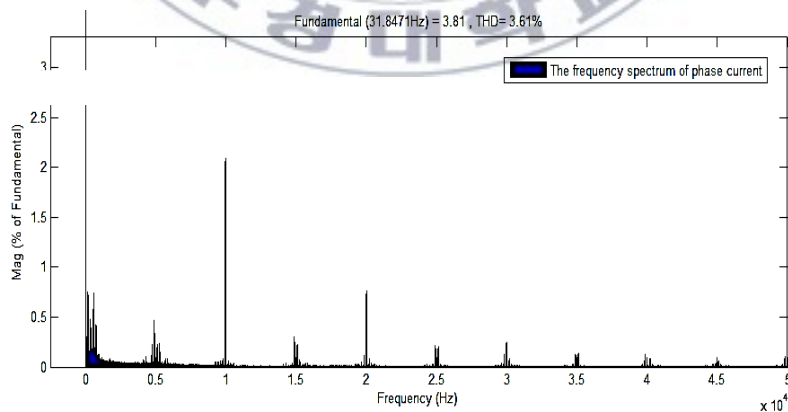Figure 3.14 The phase current harmonic analysis using FFT for SPWM

Figure 3.15 The phase current harmonic analysis using FFT for SVPWM

3.2 Simulation design for high performance control of BLDCM

Figure 3.16 is the block diagram of dual closed-loop control system of BLDCM, which mainly includes 5 parts: main body of electromotor, speed PI controller, module of reference current, current hysteresis controller and inverter.
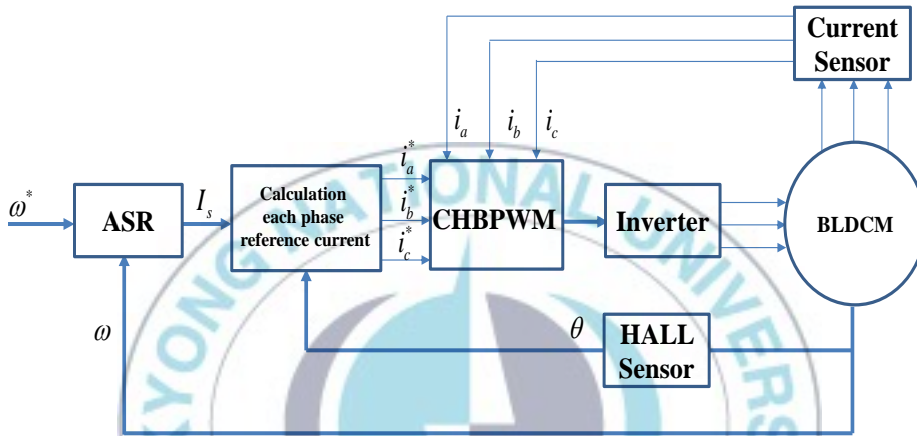

Figure 3.16 The dual closed-loop control system of BLDCM

This thesis established simulation model of BLDCM dual closed-loop control system with MATLAB/SIMULINK simulation tool and M language programming. The function and structure of each modules are described as below:

3.2.1 Simulation module of BLDCM

The simulation model of main body of BLDCM could directly call the BLDCM module in SIMULINK module database (Figure 3.16). For different BLDCM, related parameters must be set, for example pole pairs in rotor, stator windings, linkage, etc. Operation is shown as Figure 3.17.
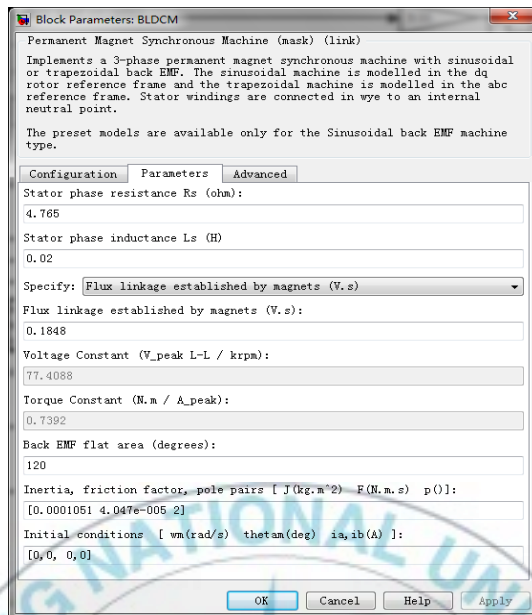
Figure 3.17 The parameters set interface of the BLDCM model

3.2.2 Speed PI controller

Applied PI controller module in SIMULINK. This module can not only set proper value of K_p and K_i, but also saturation limiting the output.

Figure 3.18 The block diagram of PI controller module

3.2.3 Reference current module

This system is applied with rotate speed & current double closed loop control system, taking the absolute value of the output I_s of speed loop as

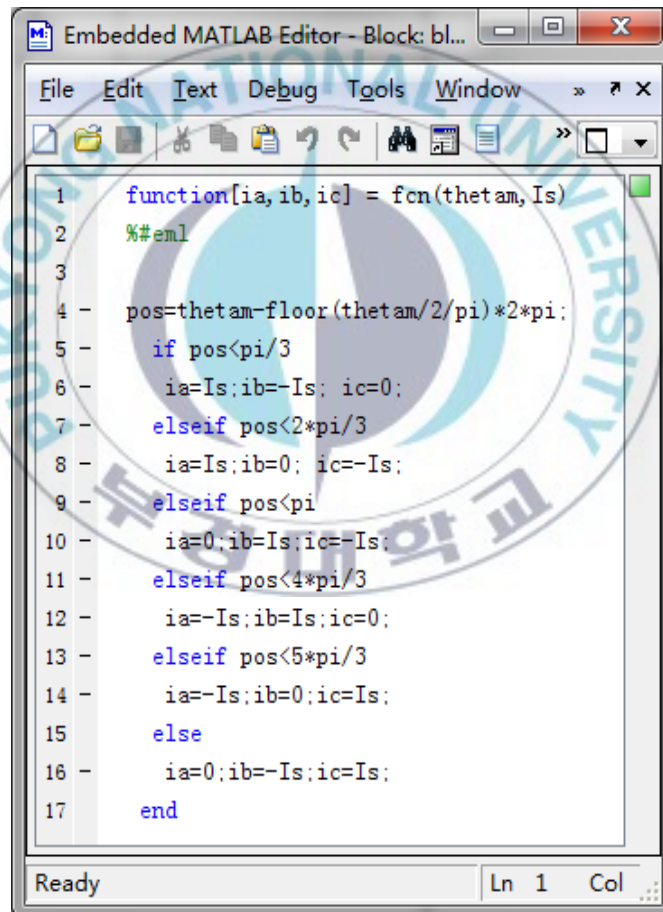reference current value. According the the feedback signal of rotor position, I_s is divided into i_a^*, i_b^* and i_c^*. Then hysteresis comparing i_a^*, i_b^*, i_c^* with feedback three phase current, so as to realize the control for current. This model could use the program coded with embedded MATLAB function in User defined functions module. The structure of program is shown as Figure 3.19. What must be explained that in actual control system, we can use three hall sensors to judge the position of rotor.


```matlab
function[ia, ib, ic] = fcn(thetam, Is)
%#eml

pos=thetam-floor(thetam/2/pi)*2*pi;
 if pos<pi/3
  ia=Is;ib=-Is; ic=0;
 elseif pos<2*pi/3
  ia=Is;ib=0; ic=-Is;
 elseif pos<pi
  ia=0;ib=Is;ic=-Is;
 elseif pos<4*pi/3
  ia=-Is;ib=Is;ic=0;
 elseif pos<5*pi/3
  ia=-Is;ib=0;ic=Is;
 else
  ia=0;ib=-Is;ic=Is;
 end
```

Figure 3.19 M program of reference current module

3.2.4 Current hysteresis control module

Three PWM signal a, c, e were got after I_s divided into i_a^*, i_b^*, i_c^* and hysteresis compared with feedback 3 phase current i_a, i_b, i_c. Other three PWM signal could be got after "not" logical operation to these three PWM signal.
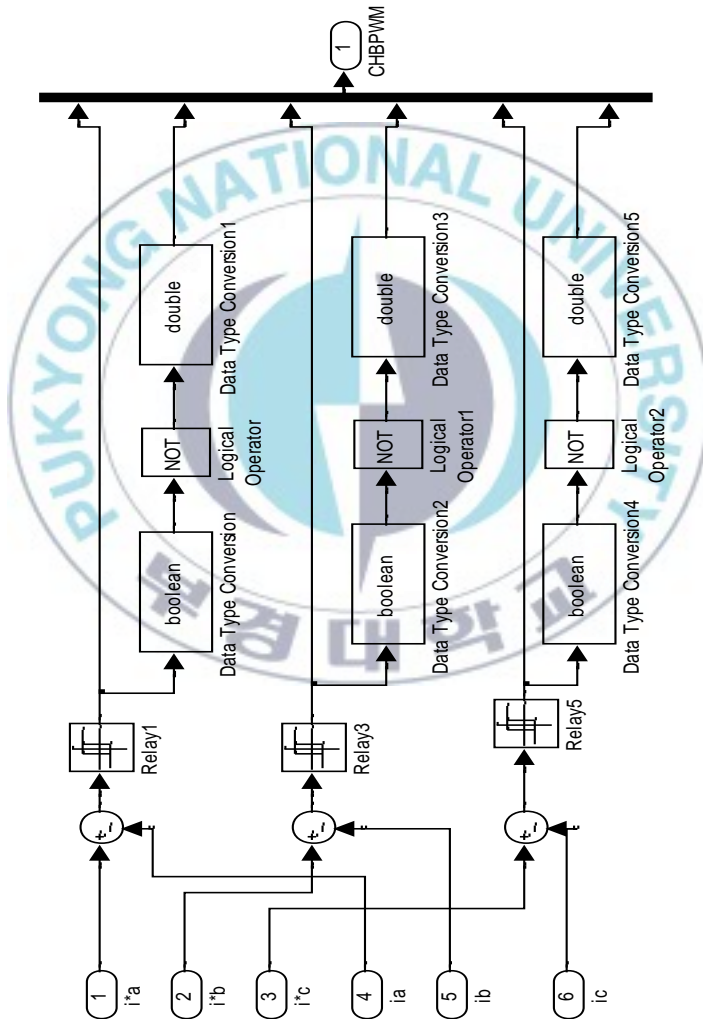

Figure 3.20 CHBPWM Control Module

3.2.5 Inverter module

Simulation model of inverter could be easily established and set related parameters by using DC power supply module and Universal Bridge inverter module of SimPowerSystem Toolbox. Shown as Figure 3.21 .
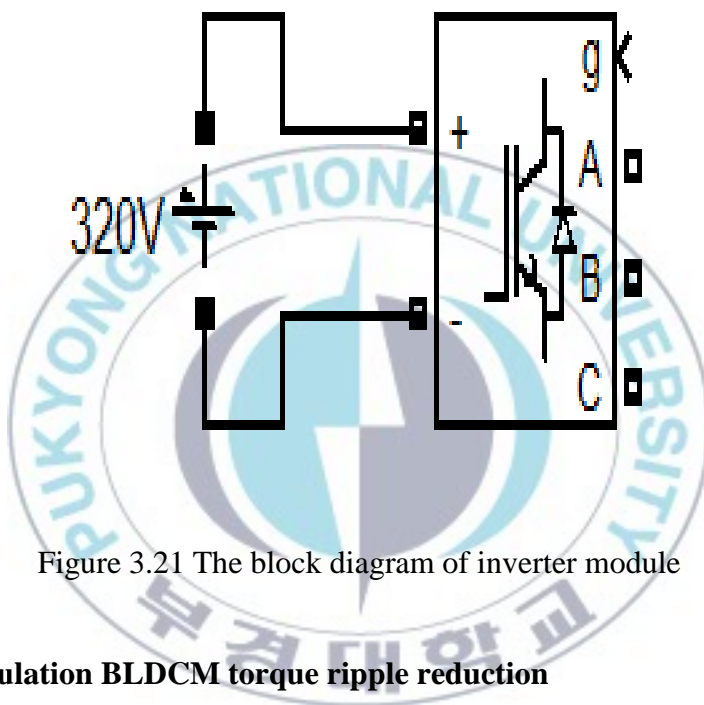
Figure 3.21 The block diagram of inverter module

3.2.6 Simulation BLDCM torque ripple reduction

Simulation models established above together contributed to simulation block diagram of BLDCM dual closed-loop control system shown as Figure 3.22.

Before simulation experiment, first, set the parameters of BLDCM. Simulation results are shown as Figure 3.23 to Figure 3.24.
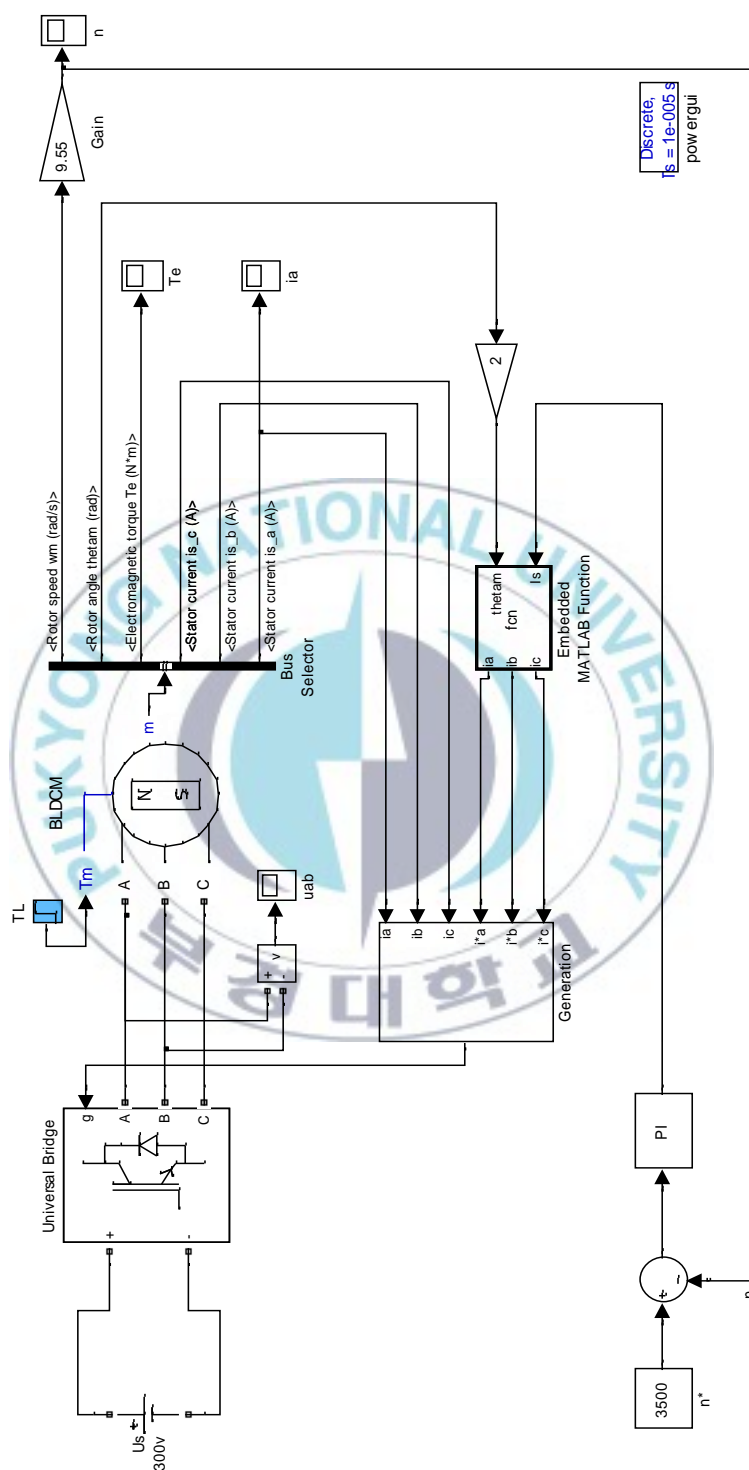
Figure 3.22 The block diagram of simulation system for BLDCM double closed loop control

63
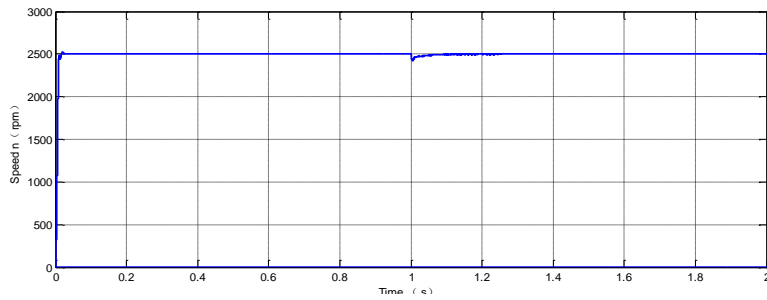
Figure 3.23 The Simulation result of speed
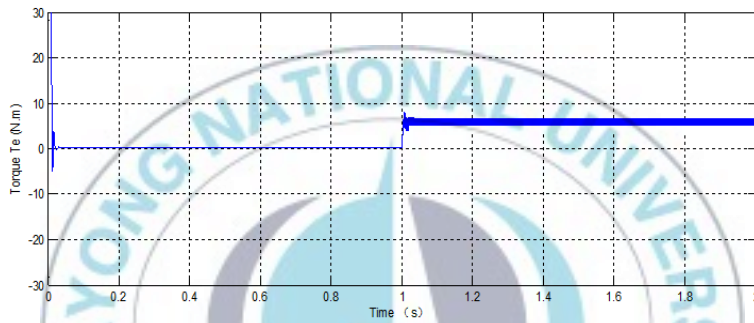
Figure 3.24 The Simulation result of torque
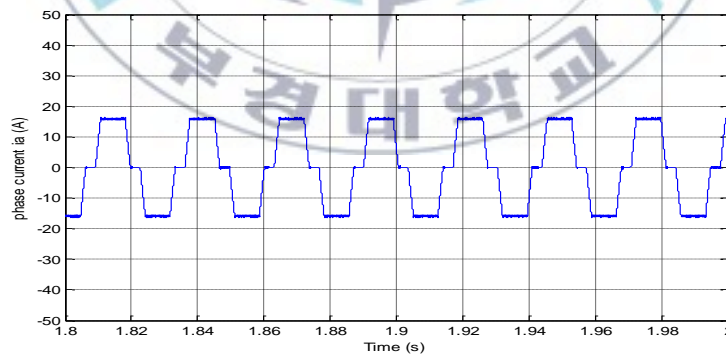
Figure 3.25 The Simulation result of phase current

Figure 3.25 is the output wave of A phase current under CHBPWM control mode. Compared with Figure 2.25, there is no noise current in A

phase current, phase current is similar to square wave. Thus the purpose is realized that reduction the torque ripple when transforming phase in BLDCM.

In this chapter, by using CHBPWM modulate mode, to have the current through windings of stator more likely to ideal square wave current, so as to effectively reduction the torque ripple when transforming phase in BLDCM, and improved the control performance of BLDCM greatly.

Chapter 4

The experiment for the vector control of BLACM

4.1 Experimental apparatus for the vector control of BLACM

The BLACM control system is composed of hardware part and software part. The hardware part contain host computer, control board (include control module, driver module, communication module, power supply module), BLACM, load torque motor, and oscilloscope, as following Figure 4.1.

Figure 4.1 The hardware set-up of BLACM vector control system

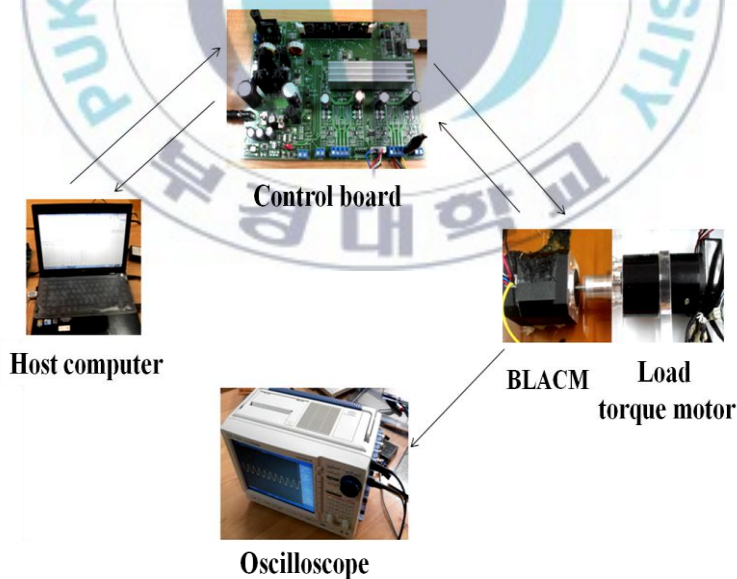Host computer supply CCStudio(Code Composer Studio) interface for programming, building, debugging, and controlling motor real time. The motor control software on control module control BLACM via driver module, and the real time status can be sampled and be sent to host computer CCStudio interface via communication module. The whole need power is generated by power module from main supply. The load torque motor supply the load torque for BLACM, and the phase current and voltage of BLACM are sampled by oscillograph.

The control board black diagram as following Figure 4.2, there are control module, driver module，communication module, power supply module. The DC-bus voltage is 24V,and three pulse width modulation (PWM) signals are from TMS320F28035.Two phase currents of the BLACM (ia and ib) are measured by shunt resistor, and are sent to the TMS320x28035 via two analog-to-digital converters (ADCs),and achieve current feedback loop. And the position and speed of rotor are measured by position sensor, and are sent to the TMS320F28035, and achieve position/speed feedback loop.

And the following Figure 4.3 is the major features of the control board which is split into several sections called macros. For example, macro [M1] is located in the upper-right hand corner of the board and is responsible for providing isolated USB emulation.[18]

The control module is based on TMS320F28035 chip, one of TMS320F2803x devices, as the processor and controller for motor control. TMS320F2803x devices are part of the family of C2000 microcontrollers which enable cost-effective design of intelligent controllers for three phase motors by reducing the system components and increase efficiency. The TMS320F28035 provides the power of the C28x core and Control Law

Accelerator (CLA) coupled with highly integrated control peripherals in low pin-count devices. It is code-compatible with previous C28x-based code, as well as providing a high level of analog integration. An internal voltage regulator allows for single rail operation. Enhancements have been made to the HRPWM module to allow for dual-edge control(frequency modulation). Analog comparators with internal 10-bit references have been added and can be routed directly to control the PWM outputs. The ADC converts from 0 to 3.3-V fixed full scale range. And the highlights as following:

- High-efficiency 32-bit CPU
- 60-MHz device
- Single 3.3-V supply
- Integrated power-on and brown-out resets
- Two internal zero-pin oscillators
- Up to 45 multiplexed GPIO pins
- Three 32-bit CPU timers
- On-chip flash, SARAM, OTP memory
- Code-security module
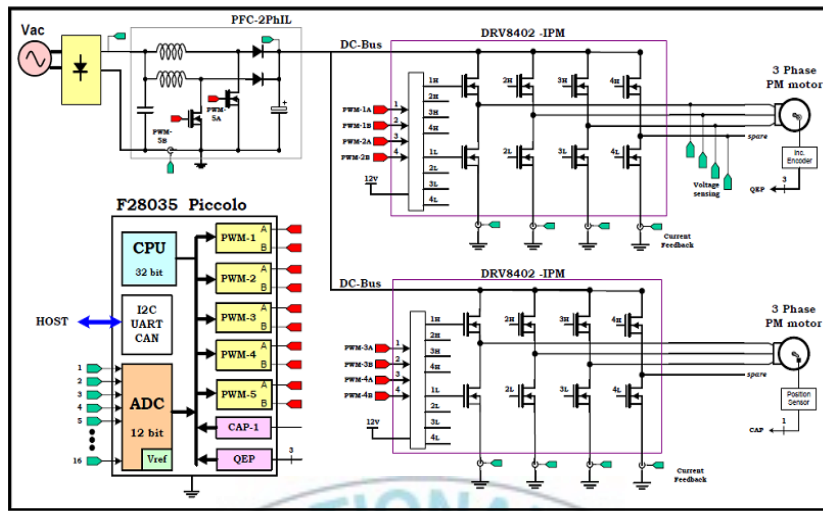- Serial port peripherals (SCI/SPI/I2C/LIN/eCAN) 、

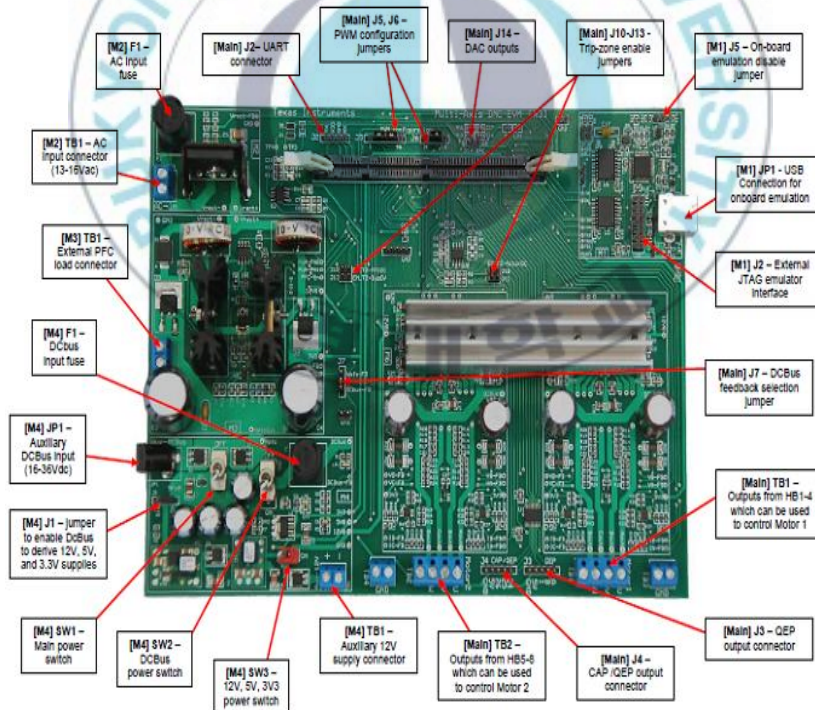Figure 4.2 The block diagram of control board

Figure 4.3 The major sections of the control board

4.2 Software design for the vector control of BLACM

The software parts contain the motor control algorithm and the program. There are two arithmetics SVPWM(Space Vector Pulse Width Modulation) and SPWM(Sinusoidal PWM) to be studied in this paper. The results will be compared to find the difference of these two algorithms.

The program is implemented by C language in CCStudio(Code Composer Studio), the tool which is developed by TI(Texas Instruments) as an integrated development environment (IDE) for Texas Instruments' (TI) embedded processor families. CCStudio comprises a suite of tools used to develop and debug embedded applications. It includes compilers for each of TI's device families, source code editor, project build environment, debugger, profiler, simulators, real- time operating system. And the version is V4. The software structure of BLACM vector control system as following Figure 4.4.
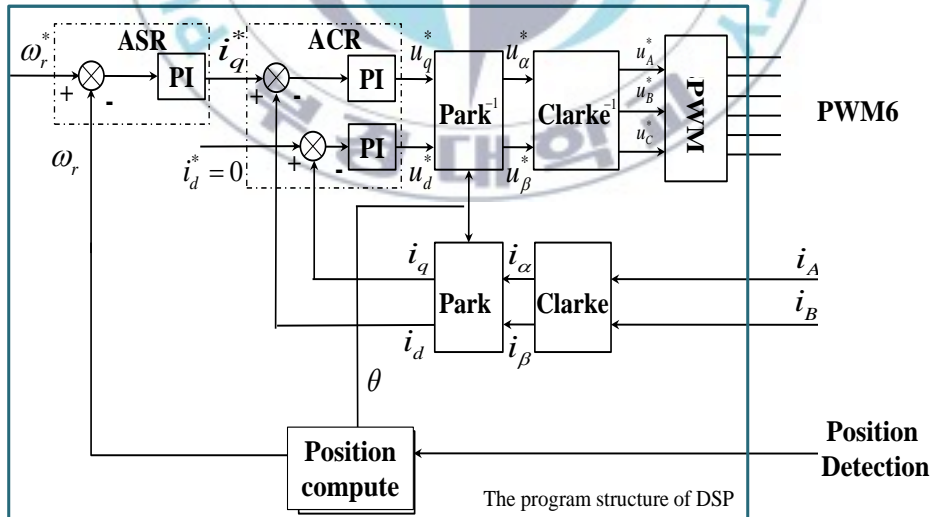

Figure 4.4 The software structure of BLACM vector control system

The BLACM vector control system software can be divided into two parts: main function and motor control function. The initialization program of main function complete the initialization of core and the peripheral units, the initialization of variables and parameters, and the initial rotor position detection of the BLACM. The background program of main function completes the management of program parameter and I/O. There are three interrupt programs in motor control function: Timer T_1 underflow interrupt, optical encoder zero pulse capture interrupt and power protection interrupt. The Timer T_1 underflow interrupt program complete the sample handling of feedback variable, vector control, double-loop (current, speed) adjustment control, PWM signal generation and the processing of soft faults. The T_1 underflow interrupts program flow chart as shown in Figure 4.5.
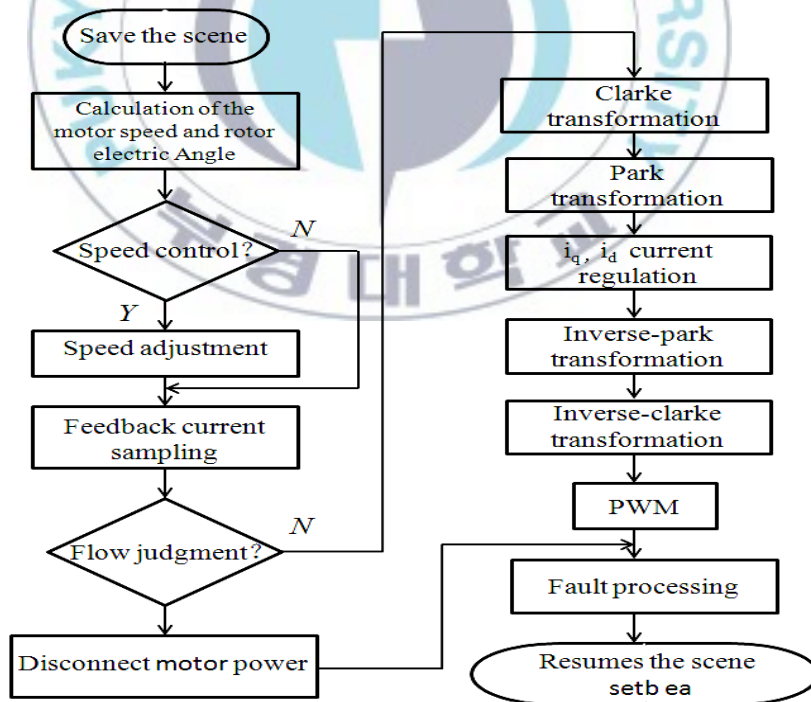

Figure 4.5 The flow chart of T_1 underflow interrupts program

For the programming of SPWM and SVPWM, refer to chapter 2 for detailed PWM principle. With T_1 programming tool CCS4, writing C programs, refer to appendix.

4.3 Experimental result and analysis

According to the experiment equipment and software which are studied above, completed two types PWM (SPWM and SVPWM) vector control experiments respectively, analyzed and compared the results.

With the same equipments and set-up, the same motor initialization setting, set the same motor speed and the initial load torque. The BLACM parameters as the following Table 4.1.

Table 4.1 The parameters of BLACM

Rated Voltage	36 V
Rated Center	1.3A
Rated Power	46 W
Rated Speed	4000 rpm
Peak Torque	0.387 Nm
Pole pairs	4

4.3.1 The experimental results of vector control

Control the motor work at speed 300rpm, 1600rpm, 2500rpm, which means the motor work at low, medium and high speed. The experimental results as following Figure 4.6, Figure 4.7, Figure 4.8 and Figure 4.9. X-axis coordinate is the sampling points. Y-axis coordinate is the speed (rpm) value and i_q (A) value.

From the equation (2-9), the motor pole pairs and the flux of rotor are constant, so the stability of i_q waveform can be used to reflect the performance of the motor torque control.

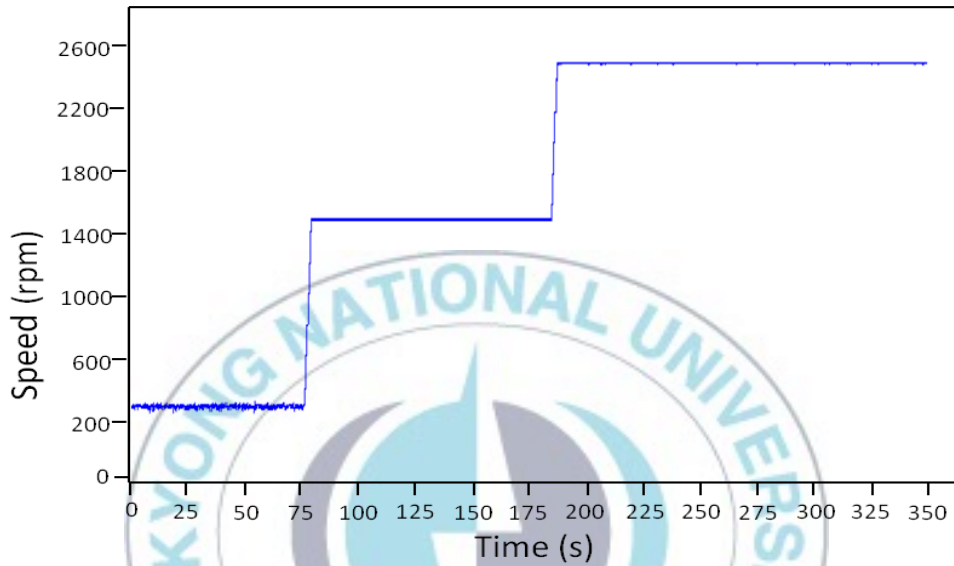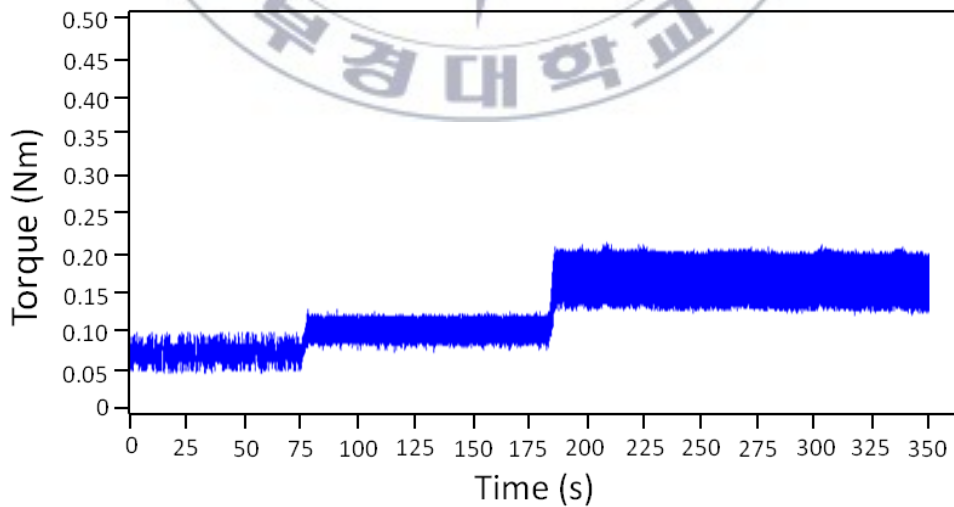Figure 4.6 The speed of SPWM vector control

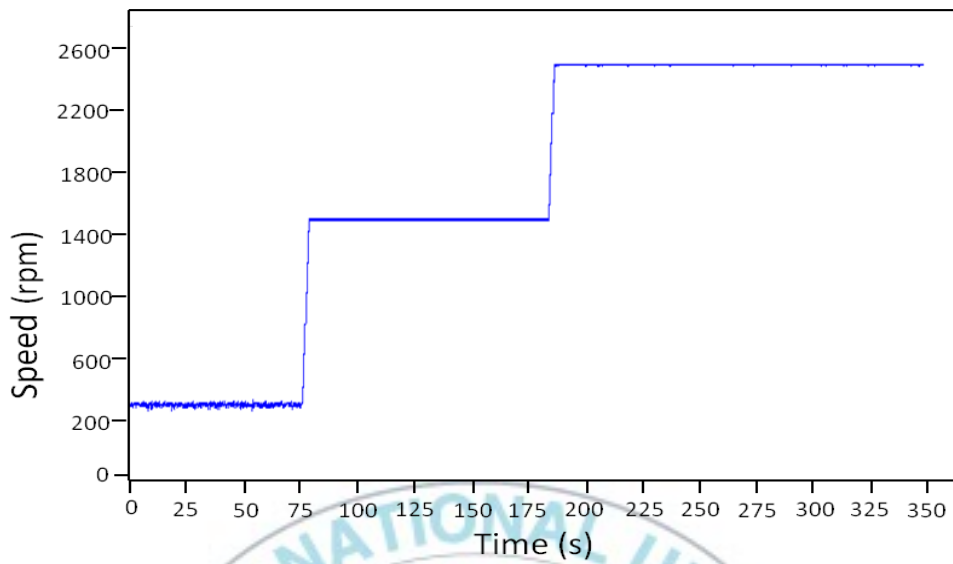Figure 4.7 The i_q of SPWM vector control

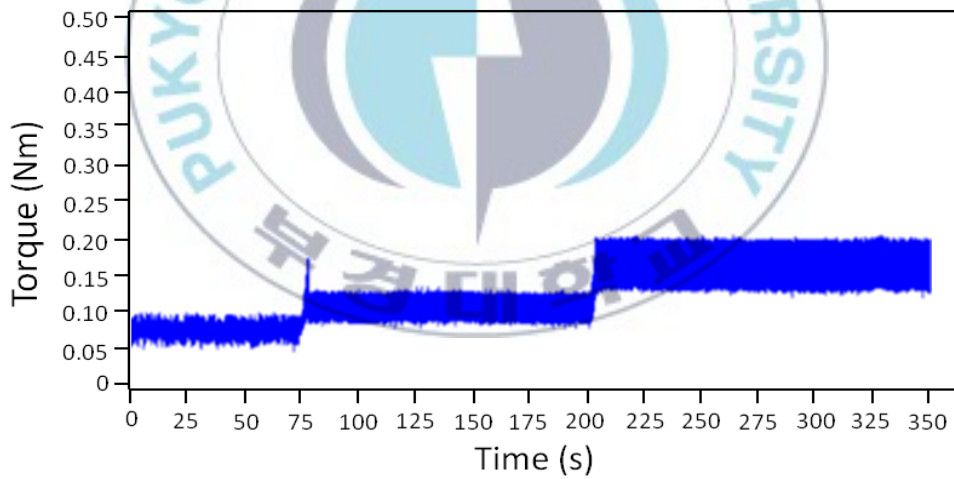Figure 4.8 The speed of SVPWM vector control

Figure 4.9 The i_q of SVPWM vector control

The reason of the ladder-like waveform in Figure 4.7 and Figure 4.9 are that load torque is provided by the load motor, and its value is not a constant, becoming bigger when the motor speed increasing. From Figure 4.6, Figure

74

4.7, Figure 4.8 and Figure 4.9, the fluctuations of speed and iq at speed 300rpm is a little larger than at speed 1600rpm and 2500rpm. It indicates that there is more high performance for BLACM at medium speed and high speed with vector control algorithm.

From Figure 4.6, Figure 4.7, Figure 4.8 and Figure 4.9, the experimental results of SVPWM algorithm are similar with the results of SPWM, and it is coincident with simulation results in chapter 3, so made the following experiment to compare the performance of SPWM and SVPWM.

4.3.2 The analysis of line voltage waveform

With Japanese YOKOGAWA DL750 waveform recorder, sample the line voltage wave for two PWM control arithmetic as shown in Figure 4.10, Figure 4.11. It is obvious that the switch density of SVPWM control arithmetic is lower than SPWM control arithmetic, thus lower switching loss. It is coincident with the simulation result in chapter 3.

The more power tube (IGBT, MOSFET) switch times per unit time, the more switch loss, the shorter life time. Therefore, this SVPWM advantage is important in practice system.

Figure 4.10 The line voltage wave for SPWM control arithmetic

Figure 4.11 The line voltage wave for SVPWM control arithmetic

4.3.3 The analysis of phase current waveform

The phase current waves of two PWM control arithmetic with DL750 as following Figure 4.12 and Figure 4.13, Compare above two figures, the difference is tiny, and analyze the phase currents data with FFT, as following Figure 4.14 and Figure 4.15.
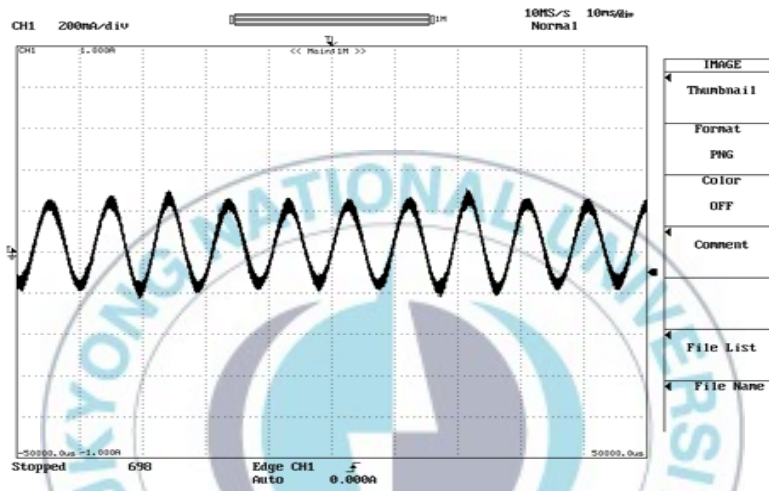

Figure 4.12 The phase current wave for SPWM control arithmetic
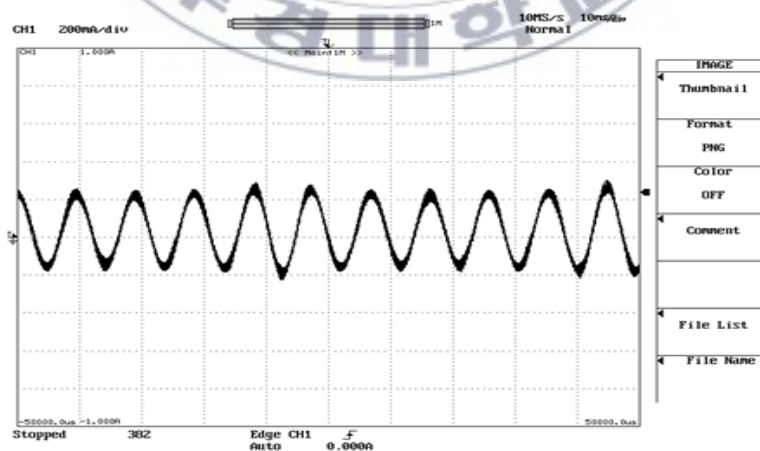
Figure 4.13 The phase current wave for SVPWM control arithmetic

From above FFT（Fast Fourier Transform） analysis results, the THD value of phase current with SVPWM control arithmetic is smaller than SPWM control arithmetic, thus the harmonic parts of phase current with SVPWM control arithmetic is more smaller. It is coincident with the simulation result in chapter 3.

The main damage of too high harmonic part to motor is the increase of power loss, the reduce of efficiency, along with the temperature rise, increased motor noise, even destroy the motor when harmonic part is more higher.

Figure 4.14 The phase current harmonic analysis using FFT for SPWM

Figure 4.15 The phase current harmonic analysis using FFT for SVPWM

Chapter 5

Conclusion

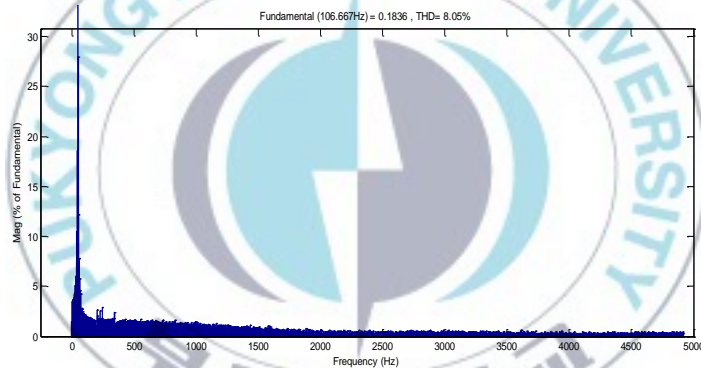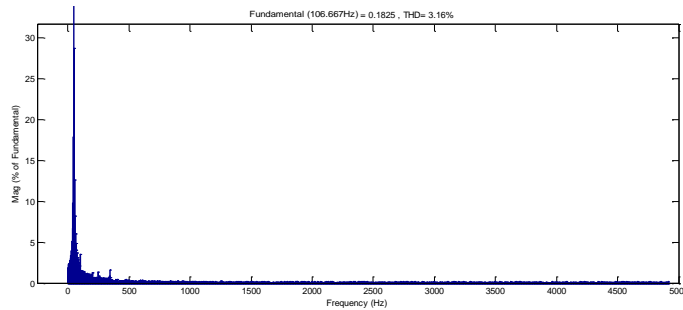For PMSM advantages, it is widely used in numerically controlled machine tools field, fire control field, aerospace field, and so on. In this paper, the present situation of PMSM control are summarized and generalized based on consulting lots of literature. First introduce the principle of rotor flux-orientation vector control for BLACM, and decoupling control for BLACM with SPWM and SVPWM technology. Second, introduce the method to reduce torque ripple with application of CHBPWM inverter based on studying the structure and control algorithm of BLACM, and complete the MATLAB/SIMULINK simulation. Last, Complete BLACM vector control experiments based on DSP TMS320F28035.The experiment result is coincident with simulation.

From the experiment that already done, some conclusions can be made as follows:

1. From the experiment, the control performance of BLACM vector control algorithm is excellent, even comparable with the control performance of DC motor. And summed up the control performance of BLACM vector control algorithm is better at medium speed and high speed than at low speed.

2. From the experiment，by comparing the line voltage waveforms of SPWM and SVPWM control algorithm, there is less switch loss with SVPWM control algorithm. It is very important in the real system.

3. From the experiment，by comparing the FFT analysis results of phase

current with SPWM and SVPWM control algorithm, SVPWM has better harmonic suppression effect.

4. From equation (2-15) and equation (2-29), the amplitude of SVPWM inverter output line voltage is same as the DC bus voltage, so DC power utilization rate was increased 15% than SPWM.

5. Through the analysis of the simulation result, CHBPWM inverter can effectively reduce the torque ripple of BLDCM, and dual closed-loop control algorithm also greatly can make improvement of the BLDCM control performance.

Acknowledgement

At the completion of my graduation thesis, I wish to express my sincere appreciation to all persons who have helped me during the past two years of my undergraduate study in mechatronics engineering of pukyong national university.

Firstly, I would like to express my heartfelt gratitude to my supervisor, Professor Seok-Kwon Jeong，for his priceless help and care throughout my master study. I appreciate his spirit of enterprise, his vast knowledge in many areas, and his assistance in writing paper. Without his consistent and illuminating instruction, this thesis could not reached its present form.

Secondly, I should give my hearty thanks to all members of my thesis committee: Professor Joo-Ho Yang and Professor Ji-Sung Jang, for their helpful comments and suggestions.

I also owe my sincere gratitude to my friends all members of AMCL Lab, for giving me a comfortable and active environment to achieve my study.

Last but not least, my thanks would go to my beloved family for their loving considerations and great confidence in me all through these years.

Sun Quanbin

References

[1]   Peter Vas, Vector Control of AC Machines, New York, Oxford University Press, 1990.

[2]   Peter Vas, Sensorless Vector and Direct Torque Control, New York, Oxford University Press, 1998.

[3]   Wang ChengYuan, Xia JiaKuan, Sun YiBioa, Modern Control Technique of Electric Machines, Beijing, China Machine Press, 2008.

[4]   Pillay P., Krishnan R. Modeling, simulation, and analysis of permanent-magnet motor drives, Part Ⅱ: The brushless DC motor drive [J]. IEEE Trans. on Industry Applications, 1989, 25（2）: 274-279.

[5]   Hong NaiGang, Power electronics, Motor control system modeling and simulation, Beijing, China Machine Press, 2010.

[6]   Jeong Y, Lorenz R D, Jahns T M, Sul S K. Initial rotor position estimation of an interior permanent magnet synchronous machine using carrier-frequency injection methods[J]. IEEE Trans. on Industry Applications, 2005, 41(1): 38-45.

[7]   Tang RenYuan, Modern Permanent Magnet Machines Theory and Design, Beijing, China Machine Press, 1997.

[8]   Degner M W, Lorenz R D. Using multiple salieneies for the estimation of flux, position, and velocity in AC maehines[J]. IEEE Transactions on Industry Applications, 1998, 34 (5) :97-104.
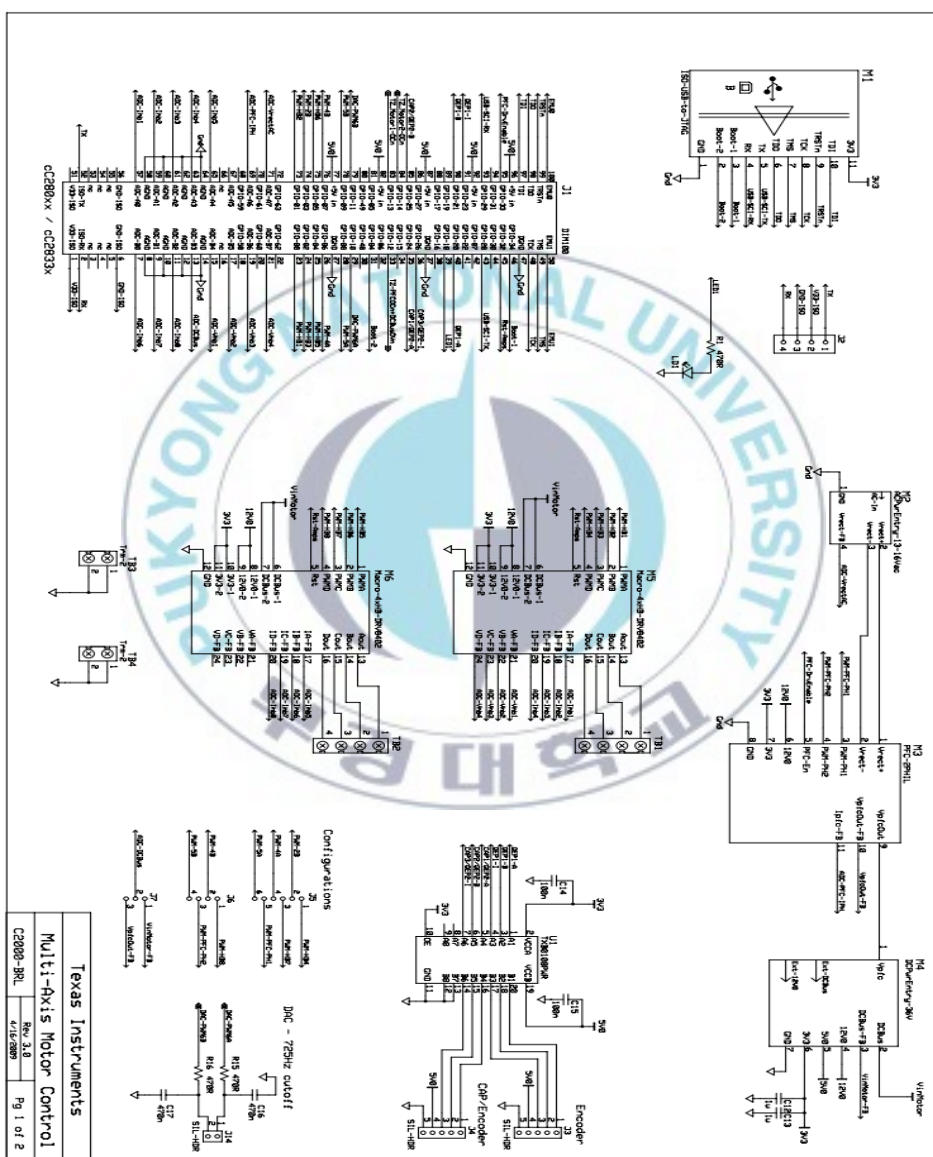
[9]   UTKIN V, LEE H. Chattering Problem in Sliding Mode Control System[J]. Variable Structure System, 2006(1): 346-350.

[10]   Ke Song, Wei guo Liu, "BLACM Field Oriented Control and HIL Simulation", IEEE Vehicle Power and Propulsion Conference, Harbin, 2008, pp. 4~6.

[11]   CHENG Min-Jun, "Research of high performance magnetism synchronous motor vector velocity modulation system", Master thesis in Zhe Jiang Industrial University, 2006, pp. 65~67.

[12]   R. Fierro, and F. L. Lewis, "Control of a Nonholonomic Mobile Robot Using Neural Networks", IEEE Transactions on Neural Networks, Vol. 9, No. 4, pp. 589-600, 1998.

[13]   Wook-Jin Lee, Seung-Ki Sul. A New Starting Method of bldc Motors without Position Sensor, IEEE Tran. Industrial Electronics, 2004, (4): 2397-2402.

[14]   Q.B. Sun, T.Y. Jeong, S.K.Jeong, A Simple Vector Control Algorithm for BLACMs, The Korean Society for Power Engineering(2011), pp.201-206

[15]   Masatoshi Hatano, Mamoru Minami, Tsuyoshi Ohsumi and HarukiObara, Modeling of Mobile Manipulators on irregular terrain and Evaluation of Disturbance Torques Department of Mechatronic Engineering, Proceeding of the IEEE/ASME International Conference on Advanced Intelligent Mechatronics, Italy, 2001.

[16]   Liang Yan, Li Yongdong. Sensorless control of synchronousmotors based on MRAS method and initial position estimation[C]. The
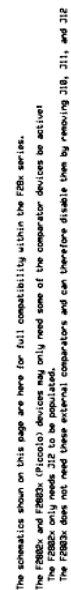
Sixth Conference on Electrical Machines and Systems 2003, l: 96—99.

[17]   Miller T J E. Brushless Permanent-Magnet and Reluctance Motor Drives [M]. Oxford New York: Clarendon Press, 1989.

[18]   LVMultiAxis+PfcKit_HWGuidev1.1 of TI DSP

[19]   Summers T, Betz R. Dead-time issues in predictive current Control [C]. Pittsburgh: Records of Industry A applications So-ciety Annual Meeting, 2002.

[20]   Urasaki N, Senjyu T, Uezato K. On-line dead time compensation method for permanent magnet synchronous motor [C]. IEEE International Conference on Industrial Technology, Bang-kok, Thailand, 2002.

[21]   Karl Johan A strom, Tore Hagglund. The future of PID control [J]. Control Engineering Practice, 2001, 9 (11).

[22]   Faa2 Jeng Lin, Sheng- Lyin Chiu, Kuo-Kai Shyu. A daptive control of PM synchronous motor drive using VSS approach [J]. Proceedings of the 1996 IEEE IECON 22nd International Conference on Industrial Electronics, Control, and Instrumentation on, 1996.

Appendix

The schematic of control board：

Vrect+

Vrect-FB
(R.63 Vacrect * 1.41Vadc)

Vrect-

13V to 16V AC-RMS (for 24V DcBus)

TB1
Txer2

F1
Fuse

D1
GBJ1504-BP

C1
220n

C2
220n

R1
75K

R2
75K

R3
10K

C3
1n

GND

Texas Instruments
Macro-DCPwrEntry-36V
C2000 – BRL   Rev.1.0   Page 1 of 2
12/16/2008

90